

See discussions, stats, and author profiles for this publication at: <https://www.researchgate.net/publication/388897532>

# A survey of intracranial aneurysm detection and segmentation

Article in *Medical Image Analysis* · February 2025

DOI: 10.1016/j.media.2025.103493

---

CITATIONS

2

READS

70

5 authors, including:



Monique Meuschke

Otto-von-Guericke University Magdeburg

83 PUBLICATIONS 770 CITATIONS

[SEE PROFILE](#)



Alejandro F Frangi

The University of Manchester

896 PUBLICATIONS 34,304 CITATIONS

[SEE PROFILE](#)



Bernhard Preim

Otto-von-Guericke University Magdeburg

770 PUBLICATIONS 9,264 CITATIONS

[SEE PROFILE](#)



Kai Lawonn

Friedrich Schiller University Jena

181 PUBLICATIONS 2,028 CITATIONS

[SEE PROFILE](#)



## Survey paper

## A survey of intracranial aneurysm detection and segmentation



Wei-Chan Hsu <sup>a</sup>\*, Monique Meuschke <sup>b</sup>, Alejandro F. Frangi <sup>c</sup>, Bernhard Preim <sup>b</sup>, Kai Lawonn <sup>a</sup>

<sup>a</sup> Friedrich Schiller University Jena, Faculty of Mathematics and Computer Science, Ernst-Abbe-Platz 2, Jena, 07743, Thuringia, Germany

<sup>b</sup> Otto von Guericke University Magdeburg, Department of Simulation and Graphics, Universitätsplatz 2, Magdeburg, 39106, Saxony-Anhalt, Germany

<sup>c</sup> University of Manchester, Christabel Pankhurst Institute, Schools of Engineering and Health Sciences, Oxford Rd, Manchester, M13 9PL, Greater Manchester, United Kingdom

## ARTICLE INFO

## Keywords:

Intracranial aneurysms  
Ostium  
Digital subtraction angiography (DSA)  
Computed tomography angiography (CTA)  
Magnetic resonance angiography (MRA)

## ABSTRACT

Intracranial aneurysms (IAs) are a critical public health concern: they are asymptomatic and can lead to fatal subarachnoid hemorrhage in case of rupture. Neuroradiologists rely on advanced imaging techniques to identify aneurysms in a patient and consider the characteristics of IAs along with several other patient-related factors for rupture risk assessment and treatment decision-making. The process of diagnostic image reading is time-intensive and prone to inter- and intra-individual variations, so researchers have proposed many computer-aided diagnosis (CAD) systems for aneurysm detection and segmentation. This paper provides a comprehensive literature survey of semi-automated and automated approaches for IA detection and segmentation and proposes a taxonomy to classify the approaches. We also discuss the current issues and give some insight into the future direction of CAD systems for IA detection and segmentation.

## Contents

1. Introduction .....	2
2. Background .....	3
2.1. Medical background .....	3
2.2. Medical imaging .....	4
2.3. Open source .....	6
3. Aneurysm detection and segmentation pipeline .....	6
3.1. Image pre-processing .....	6
3.2. Candidate detection .....	7
3.3. Post-processing .....	7
3.4. Visualization .....	7
3.5. Evaluation .....	8
3.5.1. Detection metrics .....	8
3.5.2. Segmentation metrics .....	8
4. Taxonomy .....	9
4.1. Data .....	9
4.2. Task .....	9
4.3. Methodology .....	9
4.4. Metrics .....	11
5. Approaches with 3D geometric data .....	11
5.1. Surface mesh approaches .....	12
5.1.1. Aneurysm isolation by tubular model .....	13
5.1.2. Ostium extraction .....	14
5.1.3. Shape descriptor strategy .....	14
5.1.4. DL-based methods .....	16
5.2. Point sets approaches .....	16

\* Corresponding author.

E-mail address: [wei-chan.hsu@uni-jena.de](mailto:wei-chan.hsu@uni-jena.de) (W.-C. Hsu).

5.3. Summary of geometric data approaches .....	16
6. Approaches based on volumetric data .....	16
6.1. Non DL-based methods .....	17
6.1.1. Distance analysis .....	17
6.1.2. Shape analysis .....	17
6.1.3. Deformable models .....	18
6.2. DL-based methods .....	18
6.3. Summary of volumetric data approaches .....	20
7. Approaches based on 2D images .....	20
7.1. Non-DL-based methods .....	20
7.2. DL-based methods .....	21
7.3. Summary of 2D image-based approaches .....	21
8. Discussion .....	21
9. Conclusions .....	23
CRedit authorship contribution statement .....	23
Declaration of competing interest .....	23
Data availability .....	24
References .....	24

## 1. Introduction

Intracranial (Brain/Cerebral) aneurysms (IAs) are abnormal localized dilatation of intracranial arteries due to weakened vessel wall, affecting around 3% of the adult population (Vlak et al., 2011). Most IAs are asymptomatic and are discovered incidentally during cerebral artery imaging, but they can lead to subarachnoid hemorrhage with high mortality in case of rupture. Therefore, the rupture risk assessment using imaging techniques to determine the size, location, and shape of IAs is of great importance for monitoring and treatment planning (Ishibashi et al., 2009).

Among all the imaging techniques, digital subtraction angiography (DSA) has long been considered the gold standard for IA detection because of its high spatial resolution, sensitivity, and specificity. With the development of imaging technologies, other less invasive imaging techniques, such as computational tomography angiography (CTA) and magnetic resonance angiography (MRA) have become more popular in clinical practice (Maupu et al., 2022). These imaging modalities provide radiologists with a detailed view of cerebrovascular structures to detect IAs and assess the rupture risk. Manual extraction of IAs is a tedious and error-prone process, and studies have reported a wide range of human performance, with sensitivity ranging from 0.64 to 0.90 (Mine et al., 2015; Miki et al., 2016; Bo et al., 2021; Yang et al., 2021) in CTA or MRA. Consequently, there have been many studies proposing computer-aided diagnosis (CAD) systems to automatically detect and extract morphological descriptors of IAs in various imaging modalities. CAD systems have the advantages of repeatability, objectivity, and the ability to detect tiny or heterogeneous abnormalities that humans may overlook (Ueda et al., 2019). Based on the detection algorithms, CAD systems may either directly use imaging data or accept 3D surface data reconstructed from volumetric data. The typical pipeline is shown in Fig. 1.

Over the past two decades, more than one hundred studies have been dedicated to developing CAD systems for IA detection or segmentation. Notable among these efforts are some literature reviews (El Hamdaoui et al., 2017; Marasini et al., 2022; Mensah et al., 2022) and systematic reviews (Gu et al., 2022; Din et al., 2023; Bizjak and Špiclin, 2023; Zhou et al., 2024) that have sought to consolidate findings and assess the efficacy of various methodologies. The reviews provide a great overview of the field or insights into the implication of the related studies, especially the review by Din et al. (2023) that reviewed and analyzed 43 studies published between 2004 and 2021. However, almost all the previous reviews omit the studies that employ 3D geometric data in IA detection, and focus mostly only on *deep learning* (DL)-based methodologies. We aim to provide a comprehensive survey of CAD systems for IA detection and segmentation in both

imaging and 3D geometric data, comparing the pros and cons of different methods and giving guidelines for the research topic. As most studies deal with unruptured saccular aneurysms, we mainly consider unruptured saccular IA detection or segmentation but will mention fusiform ones when necessary.

**Selection criteria.** We selected papers proposing CAD systems/methods for IA detection, isolation, or segmentation without manual annotation on IAs, i.e. semi-automated or automated methods. We do not consider papers for aortic aneurysm detection, as aortic aneurysms and IAs differ in some aspects: The structure of cerebral arteries is more complex than the structure of abdominal blood vessels (Kobashi et al., 2006). Thus, more features are required to distinguish between aneurysms and healthy vessel regions in the brain. Besides, around 90% IAs are saccular (berry-shaped), whereas 94% of aortic aneurysms are fusiform (elongated shape) (Faluk and De Jesus, 2022). Fig. 2 shows the saccular and fusiform IAs. The variation in shapes necessitates distinct morphological parameters for characterization and different methods for detecting aneurysms. Microaneurysms in 2D retinal angiography are also excluded, as the strategies for processing brain imaging and retinal angiography are quite different. We also excluded papers that segment vessels with IAs as a whole without separating them apart. As the goal of aneurysm detection is usually to obtain the size, shape, or various geometric parameters for further analysis, many papers proposed methods to quantify aneurysms or extract the ostium. A method is considered either automated or semi-automated if the user is required to intervene (e.g. clicking points on IA). Since the goal of CAD is to assist physicians in interpreting imaging data, CAD systems may require manual processes, such as parameter setting or post-processing, to initiate the procedure or further improve the diagnosis performance. We used the search engines of Google Scholar, the IEEE Xplore Digital Library, the ACM Digital Library, the Eurographics Digital Library and the PubMed. We searched using keywords with a combination of (1) intracranial/brain/cerebral aneurysm, aneurysm ostium/neck, and (2) detection, demarcation, extraction, isolation, segmentation, and quantification. Relevant papers were also searched from the references of the found papers. We also included papers whose goal was morphological analysis and rupture risk prediction as they also require IA detection or segmentation. The morphological analysis aims to measure the *morphological descriptors* of IAs, such as diameter and dome height, and composed morphological descriptors computed using two values, such as aspect ratio. These descriptors rely on accurate aneurysm quantification and are essential for rupture prediction. In this paper, we refer to intracranial aneurysms as simply aneurysms.

In summary, our contributions are:

- A comprehensive survey of literature in semi-automated or automated detection and segmentation of intracranial aneurysms.

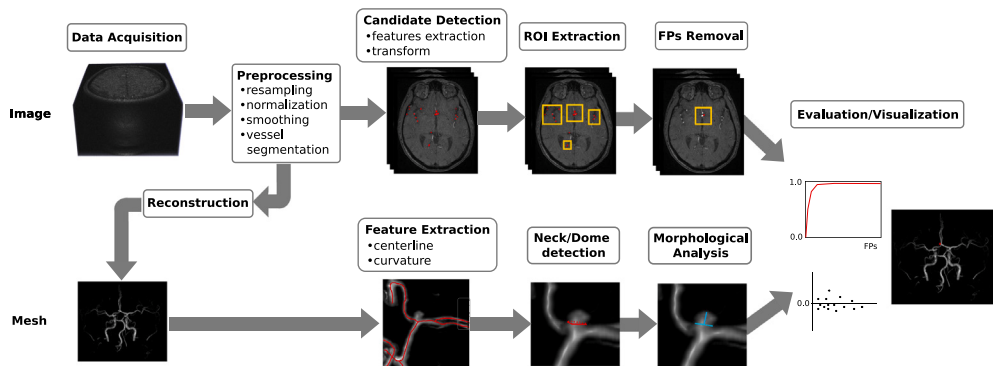


**Fig. 1.** This is a pipeline for aneurysm detection and segmentation. The top half shows the steps of image-based approaches, while the bottom half shows the steps of surface-based approaches whose input (surface mesh) is reconstructed from the segmented vasculature of a 3D volume. Surface-based approaches usually aim at morphological analysis for rupture prediction or treatment planning.

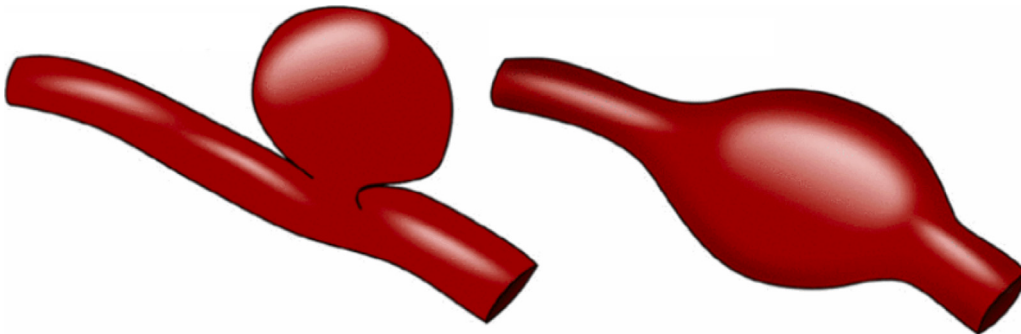


**Fig. 2.** Intracranial aneurysms (IAs) can be classified by shape: saccular (left) and fusiform (right).  
Source: Image from Meuschke et al. (2018a).

- A classification of the methods for aneurysm detection and segmentation based on the input data.
- Identifying trends and challenges in automated intracranial aneurysm detection and segmentation, offering insights into methodology evolution and future directions for research and clinical use.

**Outline.** In Section 2, we summarize the medical background of aneurysms and the imaging techniques, as well as the related data and source code that is publicly accessible. Section 3 describes the general pipeline of aneurysms detection and segmentation with some popular metrics for result evaluation. We propose a taxonomy of aneurysm detection in Section 4 based on data, task, and methodology. From Sections 5 to 7, we respectively summarize the approaches using 3D geometric data (surface mesh and point sets), volumetric data, and 2D images as input. We discuss the limitations and issues in the current aneurysm detection approaches in Section 8 and make conclusions in Section 9.

## 2. Background

This section provides the medical background of aneurysms, including their categorization, diagnosis, risk assessment, and treatment. We also briefly describe the three most typical imaging modalities and data transformation into 2D images or surface mesh. Finally, we summarize the open-source detection algorithms and publicly available aneurysm data.

### 2.1. Medical background

Aneurysms are abnormal localized dilation of intracranial arteries due to weakened vessel walls, most commonly seen in arteries.

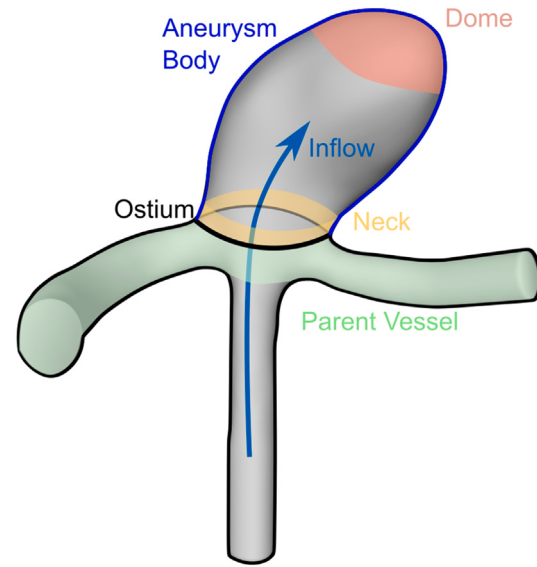


**Fig. 3.** Anatomy of a saccular aneurysm.  
Source: Image adapted from Neugebauer et al. (2010).

Aneurysms can be categorized based on their diameter (small: <5 mm, middle-sized: 5–15 mm, large: 15–25 mm, giant: 25–50 mm, and super-giant: >50 mm) and shape (saccular and fusiform). Around 90% of aneurysms are saccular in shape, commonly arising as thin-walled sacs

protruding from the arteries in the brain. Aneurysms may occur at various locations, most commonly at the *anterior communicating artery* (ACom) (35%), *internal carotid artery* (ICA) (30%) and *middle cerebral artery* (MCA) (22%) (Gasparotti and Liserre, 2005). The anatomy of a typical saccular aneurysm is shown in Fig. 3: the aneurysm is separated from its parent vessel by the ostium, which is roughly a planar section described by the neck curve. Saccular aneurysms may have a non-spherical shape and sometimes have multiple lobes (multi-lobular). Fusiform aneurysms balloon outward from the arteries on all sides and occur mostly at the middle cerebral artery and internal carotid artery (Park et al., 2008). The prevalence of aneurysms is around 3% in the general population (Vlak et al., 2011), but the real percentage is unknown because most aneurysms are asymptomatic and are incidentally discovered during neuroradiological examinations. 20% to 30% of the patients exhibit multiple aneurysms (Weir, 2002). Aneurysms typically develop between the age of 40 and 60 and are more prevalent among females. The formation of aneurysms is not fully understood but is known to be associated with hemodynamically induced degenerative vascular changes. Risk factors include hypertension, smoking, family history of aneurysms, or autosomal dominant polycystic kidney disease (Etmian and Rinkel, 2016).

Aneurysms require imaging examinations to be detected and diagnosed. Imaging techniques include *digital subtraction angiography* (DSA), *computed tomography angiography* (CTA), *magnetic resonance angiography* (MRA), *transcranial Doppler sonography* (TDS) (Turner and Kirkpatrick, 2000), and *optical coherence tomography* (Liu et al., 2019; Ku et al., 2022) (OCT). DSA has long been considered the gold standard of aneurysm detection due to its high resolution, sensitivity, and specificity (Turán et al., 2018). However, DSA only provides a single projection of the vessel structure and may fail to detect an aneurysm if the lesion overlaps nearby vessels. 3D (rotational) DSA or *3D rotational angiography* (3DRA) not only provides an additional dimension to avoid interpretation errors from occlusions of vascular structures but also improves the spatial resolution of DSA with higher sensitivity of detecting small aneurysms (Wong et al., 2012). Compared to 3DRA, CTA, and MRA do not require the invasive insertion of a catheter while providing a comparable 3D representation of the vascular anatomy. As OCT and TDS are rarely used to detect IAs and have not been applied to automated aneurysm detection, we will not cover these modalities in this paper.

The primary risk of aneurysms is rupture, which results in subarachnoid hemorrhage (SAH). SAH accounts for 5% of all stroke types (Van Gijn et al., 2007) with high mortality and morbidity. With more rapid detection and improved treatment strategies, the mortality rate has decreased during the last few decades, but recent studies still reported a 30-day mortality rate of around 20%–40% (Worthington et al., 2017; Asikainen et al., 2023; Labuz-Roszak et al., 2022). The rupture of aneurysms is associated with several factors, including the location, size, and shape of the aneurysms. For instance, basilar tip aneurysms have a higher rupture risk than other aneurysms (Al-Sharydah et al., 2021). Larger aneurysms generally have a higher rupture risk, but studies showed that most ruptured aneurysms were middle-sized (5–10 mm) (Wermer et al., 2007). The more deciding factors are the growth rate and the hemodynamics within the aneurysm. A concentrated inflow jet with a small impingement zone increases the risk of rupture (Cebral et al., 2011). The blood flow within an aneurysm is affected by the aneurysm geometry, and one widely used measure is the aspect ratio, where 1.18 is the threshold value above which aneurysms are considered dangerous (Dhar et al., 2008). Another promising morphological descriptor for risk assessment is the aneurysm angle. In clinical practice, the morphological descriptors are estimated by clinicians in 3D angiographic images, in which either a cutting plane is manually placed or the contour is drawn around the aneurysm neck. The cutting plane results in a less accurate yet more repeatable measurement because of a lower degree of freedom (Jerman et al., 2019).

To manage aneurysms, there are two intervention strategies: *endovascular coiling* and *surgical clipping* (Fig. 4). The coiling procedure is guided by fluoroscopy using a catheter from the femoral artery to the cerebral vasculature via the internal carotid or vertebral artery. As the catheter reaches the aneurysm, soft platinum coils are deployed in the lumen of the aneurysm to completely fill the lumen and induce the formation of clotting (embolization) to occlude the aneurysm and prevent rupture. The clipping procedure involves placing a surgical clip at the junction of the parent vessel and the neck of the aneurysm (Keedy, 2006). Coiling is safer than clipping, which requires neurosurgery, but applies only to saccular aneurysms with a narrow neck and can result in thrombus recanalization, leading to a rupture risk and needs more following coiling procedures (higher recurrence rate). Clipping is relatively more effective but is associated with a higher risk of complications. Hence, comparing the rupture risk and the risks associated with an intervention is necessary. The PHASES score (Greving et al., 2014), calculated by six factors (population, hypertension, age, size of aneurysm, earlier SAH from another aneurysm, site of aneurysm), provides a way to predict the aneurysm rupture risk and may be used for treatment decision. Given that most aneurysms are stable, i.e. their geometry and the blood flow stay constant over time, a valid strategy for initially low-risk aneurysms is to observe these asymptomatic aneurysms over time in medical imaging.

## 2.2. Medical imaging

Medical imaging plays a critical role in all stages of the management of aneurysms, including initial screening, diagnosis, risk assessment, treatment decision, and follow-up after treatment. DSA and 3DRA are often utilized for treatment planning and intraoperative guidance, providing detailed vascular anatomy information. Conversely, CTA and MRA are commonly employed for screening and diagnosis purposes, offering non-invasive imaging modalities for initial assessment and follow-up evaluations. We will have a comprehensive overview of different image modalities for aneurysm management. Table 1 provides a summary of the pros and cons of the three main modalities as well as their common usages. 3D rotational angiography (3DRA) shares a close technical similarity with computed tomography angiography (CTA) due to both modalities employing cone beam computed tomography (CBCT) techniques for volumetric imaging. Despite this similarity, we adhere to the conventional viewpoint found in the literature by discussing 3DRA alongside digital subtraction angiography (DSA). A more detailed comparison of imaging of aneurysms can be found in Yoon et al. (2016), Maupu et al. (2022) and Beaman et al. (2023).

**Digital subtraction angiography (DSA).** DSA is a fluoroscopic technique using X-rays to visualize blood vessels. The procedure involves the insertion of a catheter into an artery in the leg passing to the intracranial vessels to inject the contrast agent. After contrast injection, a DSA image is obtained by subtracting a mask (pre-contrast) from the image. The contrast images are taken in sequence while the contrast agent is being injected, allowing DSA to acquire both spatial and temporal information. DSA is considered the gold standard for aneurysm diagnosis for its high resolution of 0.2 mm or less (Spuler and Goubergrits, 2020), allowing the detection of small aneurysms. DSA can also acquire hemodynamic information of vessels such as collateral flow and flow direction (Stafa and Leonardi, 2008), which is important for treatment planning. 3DDSA and 3DRA enhance the diagnostic capability of 2D DSA by reconstructing 3D tomographic images. 3DRA requires a single rotational scan, while 3DDSA requires two rotations (one without contrast and one with contrast). These 3D modalities provide a clearer view of complex vascular structures, avoiding interpretation errors caused by overlapping vessels and enabling detailed aneurysm shape analysis. However, DSA is invasive, relatively expensive, and associated with complications, so it is less used for follow-up.

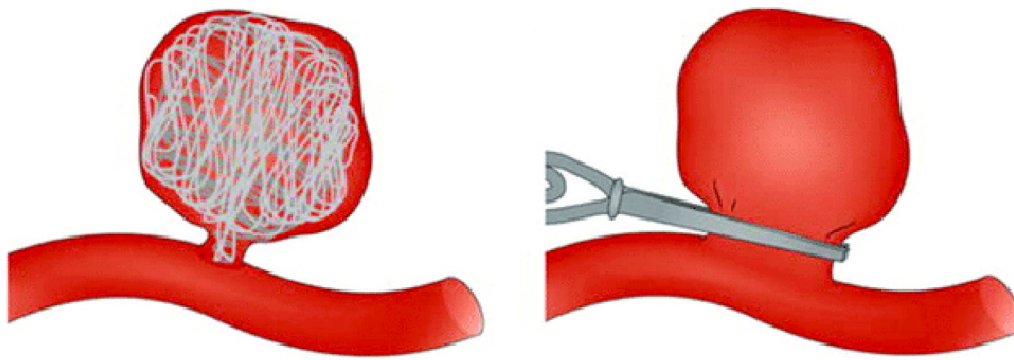


**Fig. 4.** Endovascular coiling (left) and surgical clipping (right) are the two aneurysm treatment strategies.  
Source: Image from Ngeope et al. (2018).

**Table 1**  
Comparison of imaging modalities for aneurysm analysis.

Modality	Pros (+) & Cons (-)	Observations
DSA	<ul style="list-style-type: none"> <li>+ High spatial resolution</li> <li>+ Spatial and temporal info</li> <li>+ Can acquire hemodynamic info</li> <li>- Iodinated agent required</li> <li>- Invasive</li> <li>- Radiation exposure</li> </ul>	<ul style="list-style-type: none"> <li>• Gold standard</li> <li>• Clinical usage: diagnosis, treatment planning</li> <li>• Resolution: 0.2 mm</li> </ul>
3DRA	<ul style="list-style-type: none"> <li>+ Similar advantages as DSA</li> <li>+ 3D view (better than DSA)</li> <li>- Similar disadvantages as DSA</li> </ul>	<ul style="list-style-type: none"> <li>• Clinical usage: diagnosis, treatment planning</li> <li>• Most commonly used modality for surface reconstruction</li> <li>• Resolution: 0.11–0.3 mm</li> </ul>
CTA	<ul style="list-style-type: none"> <li>+ Fast acquisition</li> <li>+ Non-invasive</li> <li>+ Can detect calcifications and thrombus</li> <li>- Iodinated agent required</li> <li>- Radiation exposure</li> <li>- Relatively low contrast between structures</li> </ul>	<ul style="list-style-type: none"> <li>• Clinical usage: (hemorrhage) screening, follow-ups</li> <li>• Often used for segmentation</li> <li>• Variant: DE-CTA, subtraction CTA, mCTA</li> <li>• Resolution: 0.35–0.7 mm</li> </ul>
MRA	<ul style="list-style-type: none"> <li>+ Non-invasive</li> <li>+ No radiation exposure</li> <li>- High cost</li> <li>- Long scan time</li> <li>- Low spatial resolution</li> <li>- Prone to several artifacts</li> </ul>	<ul style="list-style-type: none"> <li>• Clinical usage: screening, follow-ups</li> <li>• Most commonly used modality in the literature</li> <li>• Usually used for detection</li> <li>• Variants: CE-MRA, PC-MRA, TOF-MRA</li> <li>• Resolution: 0.4–1.0 mm</li> </ul>

**Computed tomography angiography (CTA).** CTA is acquired using a rotating X-ray tube and a row of detectors to measure attenuated X-ray signals in the Hounsfield unit (HU). With the injection of iodine contrast from the vein in the arm, the vessels in the brain can be enhanced to have a value around 150–375 HU (Hentschke et al., 2014). The introduction of multidetector CTA decreases the imaging acquisition time. Even with a larger resolution (0.35–0.7 mm) than DSA, CTA is less expensive, less invasive, and faster to obtain. Dual-energy CTA (DE-CTA) is a relatively new imaging technique involving simultaneous or near-simultaneous acquisition of two sets of CT imaging using different energy spectra. It can differentiate between materials with similar HU and thus is useful for detecting aneurysms (Howard et al., 2019). Multi-phase CTA (mCTA) comprises volume acquisitions before and during the injection of contrast agent, benefiting the diagnosis with temporal resolution (Wang et al., 2023). The ability to detect calcifications and thrombus makes CTA ideal for treatment decisions (Chappell et al., 2003).

**Magnetic resonance angiography (MRA).** MRA is a variant of magnetic resonance imaging (MRI) to visualize blood vessels. There are three techniques of MRA: contrast-enhanced (CE), time-of-flight (TOF), and phase-contrast (PC). Similar to CTA, CE-MRA relies on using a contrast agent (gadolinium). TOF-MRA is based on the principle of flow-related enhancement to emphasize blood flow without any contrast agent but is insensitive to in-plane flow. PC-MRA is another non-contrast MRA based on using bipolar gradients to encode blood flow velocity from phase shifts of the moving spins. Due to the flowing

blood, vasculature can be distinguished from other tissues. PC-MRA shows better contrast between the vessel lumen and the neighboring structures than TOF-MRA but can have fluctuating signals because of the change in blood flow velocity (Law and Chung, 2012). MRA has a lower resolution of 0.4–1.0 mm than DSA and CTA, thus a lower sensitivity for detecting small aneurysms. MRA is also prone to several artifacts, such as saturation and susceptibility artifacts.

**Data transformation.** In addition to the aforementioned imaging modalities, volumetric datasets are often transformed to 2D images by *maximum intensity projection* (MIP) or reconstructed as 3D surface models. MIP is a volume rendering technique that projects the voxels of maximum intensity onto the visualization plane. It allows clinicians to quantify aneurysms by calculating their morphological descriptors for treatment planning. 3D surface models provide a clearer view of the vascular anatomy than volumetric data since they are already preprocessed by vessel segmentation and are free from other structures with similar intensity values. Therefore, surface models are suitable for aneurysm detection as well as for quantitative analysis to measure morphological descriptors. However, surface processing has limitations due to sensitivity to beam hardening artifacts, notably in CBCT acquisitions like CTA or 3DRA, particularly at the ostium, leading to potential overestimation of the neck size. There are also methods using point sets (point clouds) from surface models for aneurysm segmentation. Unlike the typical procedure of reconstructing a surface from point clouds acquired by scanners, the vessel point sets are simply the vertices taken from the surface models. Therefore, the point data quality depends on the quality of vessel segmentation as well as the surface reconstruction.

**Table 2**  
Open source code of aneurysm detection and segmentation.

Reference	Input data	Method	Framework
Mitra et al. (2013)	2D DSA	Modified Hough Circle Transform & Peak Trekking	MATLAB
Jerman et al. (2015a)	3D, 2D angiography	Enhancement Filter	MATLAB
Shi et al. (2020)	CTA	DA-ResUNet	Python, PyTorch
Yang et al. (2021)	CTA	Attention ResNet-18	Python, PyTorch
Bo et al. (2021)	CTA	GLIA-Net	Python, PyTorch
Yu et al. (2021)	MRA	Point Transformer	Python, PyTorch
Di Noto et al. (2022)	MRA	U-Net	Python, TensorFlow
Assis et al. (2023)	MRA	3D ResNet with Localization and Orientation Head	Python, PyTorch
Cao et al. (2024b)	CTA	Reliable Weight Selection Mean Teacher (RWS-MT)	Python, PyTorch

**Table 3**  
Open source datasets for aneurysm detection and segmentation.

Dataset	Reference	Data type	Spatial resolution	Description
@neurIST	Iavindrasana et al. (2008)	3DRA	0.208–0.378 mm	The aim was to create an integrated decision support system for cerebral aneurysm management, resulting in a database of more than 300 datasets with at least one aneurysm. Soler et al. (2017) further refined this dataset by focusing on aneurysms at the MCA bifurcation, generating 50 cases in surface format. The project website and database were made inaccessible.
AneuRisk	Sangalli et al. (2014)	3DRA	-	The aim was to statistically investigate the correlation of intracranial vessel morphology and blood fluid dynamics with rupture. It contains 65 datasets suspected of having aneurysms.
CADA	Ivantsits et al. (2020a)	3DRA	0.25 mm	Cerebral Aneurysm Detection and Analysis (CADA) challenge was part of the MICCAI 2020 for aneurysm detection, segmentation, and risk assessment. It contains 109 datasets for training and 22 additional datasets for evaluation.
CMHA	Song et al. (2024)	CTA	0.450–0.488 mm	The dataset contains CTA datasets with related clinical, morphological, and hemodynamic parameters from 44 healthy controls and 99 patients with aneurysms.
ADAM	Timmins et al. (2021)	TOF-MRA	0.195–1.04 mm (in-plane), 0.4–0.7 mm (slice)	Aneurysm Detection And segMentation (ADAM) challenge was part of MICCAI 2020, with a database consisting of 113/141 TOF-MRA train/test datasets with T1, T2, FLAIR contrast.
IntrA	Yang et al. (2020a)	MRA	-	The database promotes the applications of point-based and mesh-based aneurysm classification and segmentation. A total of 1909 blood vessel segments were generated from the complete 109 models of the entire brain vessels.
OpenNeuro	Noto et al. (2022)	TOF-MRA	-	With 284 subjects with or without aneurysms, the database was provided for researchers to assess the multi-site robustness of their CAD system.

### 2.3. Open source

In this section, we summarize the open-source algorithms for aneurysm detection and segmentation, including the source code (Table 2) and the medical imaging datasets (Table 3). The source code of two studies using traditional approaches is based on MATLAB, while more recent studies proposed DL-based approaches rely on the Python frameworks. Medical data are usually inaccessible because of privacy and ethical issues. Even if the data are available, many imaging-related research tasks require time-consuming manual annotations by experienced clinicians. With the development of data-driven CAD systems using DL algorithms, there have been increasingly more anonymized medical data made available for open challenges and research purposes. We provide a summary of six open databases; however, one is now inaccessible, and some require signing a confidentiality agreement.

## 3. Aneurysm detection and segmentation pipeline

Several aneurysm detection methods have been proposed, but they follow a general pipeline for different modalities: image preprocessing (resampling, noise reduction, normalization, vessel segmentation), candidate aneurysm detection, region of interest (ROI) extraction, post-processing to remove false positives and refine the result, and finally evaluation and visualization of the result. In this section, each step will be described. Manual data annotation of aneurysm dome, ostium, location, and morphological parameters is regarded as ground truth (GT) in most of the papers. The annotation requires at least one experienced neuroradiologist who uses annotation software like ITK-SNAP to locate and segment any aneurysms, usually using DSA as the

gold standard for assessment. The geometry of the aneurysms, such as the height and width, are marked when necessary. A more detailed description of the process can be found in Park et al. (2019), Jang et al. (2020) and Shi et al. (2020). As the GT is assumed to be available with the datasets, manual annotation is not considered part of the pipeline. A general pipeline is demonstrated in Fig. 1.

The tasks of aneurysm detection and segmentation serve distinct roles: detection identifies the presence of aneurysms, while segmentation delineates the boundaries and enables the quantification of the size. However, the emergence of deep learning, particularly with architectures like U-Net, has blurred these boundaries by enabling both tasks to be addressed within a unified framework. Despite this convergence, it is crucial to acknowledge their separate contributions to clinical workflows. This section discusses the integrated yet differentiated strategies of the aneurysm detection and segmentation pipeline.

### 3.1. Image pre-processing

Image preprocessing aims to standardize the datasets, remove unwanted signals (noise), and enhance the object of interest. After acquiring 3D volumetric image data, *resampling* by linear or nonlinear interpolation is usually performed to achieve isotropic resolution so that filtering, morphological, or other further operations can be performed to obtain a uniform result. Depending on the imaging modalities or methods, various strategies may be required. Compared to DSA and MRA, CTA has a low vessel-to-background contrast, making many structures visible and visually indistinguishable. Therefore, some papers also apply *intensity clipping* (Park et al., 2019; Shi et al., 2020), smoothing (Firouzian et al., 2011), or bone removal (Chowriappa

et al., 2013) to CTA datasets. Firouzian et al. (2011) have shown that nonlinear diffusion smoothing can improve segmentation accuracy. In the case of MRA, intensity inhomogeneity (bias field) appearing as low-frequency multiplicative noise may be present due to systematic errors (e.g. radio-frequency nonuniformity, static field inhomogeneity) or patient motion (Hou, 2006). Bias field correction methods such as the nonparametric nonuniform intensity normalization (N3) method (Sled et al., 1998) can improve the image quality. As image data may be acquired from different scanners or at different times with varying settings, it is essential to apply intensity standardization or normalization, such that all the image datasets are within the same intensity range.

An additional pre-processing step is *vessel segmentation* or extraction. As aneurysms belong to the vascular structure, the extraction of vessels removes irrelevant structures and allows better aneurysm detection. Vessel segmentation is a requirement for polygonal surface reconstruction from volumetric data. The most common methods include *region growing* (Nikravanshalmani et al., 2010) and *geometric deformable models* (e.g. geodesic active regions) (Sgouritsa et al., 2010; Larrabide et al., 2011; Chowriappa et al., 2013). Region growing works by grouping adjacent pixels or voxels given some seed point and similarity criteria, while deformable models rely on the iteration of curves or surfaces by minimizing an energy function. For data with good contrast-enhanced vessels, global thresholding (e.g., Otsu's thresholding (Otsu, 1979)) or vessel enhancement filtering (e.g., Frangi filter (Frangi et al., 1998)) are implemented to obtain binary images of vascular structure. When 2D or 3D images are used for aneurysm detection, vessel segmentation is not always necessary (Hentschke et al., 2014). This is especially the case when deep neural networks are used because the networks are able to automatically extract useful features from the data. More detailed information about vessel segmentation can be found in Kirbas and Quek (2004), Radaelli and Peiro (2010), Taher et al. (2018) and Goni et al. (2022).

These pre-processing steps are also employed in papers using 2D images as input data, except for the resampling step. To reduce the computational cost and complexity, some authors chose to apply MIP to obtain 2D images as input (Nakao et al., 2018; Stember et al., 2019; Shimada et al., 2020).

### 3.2. Candidate detection

The main task of the pipeline is candidate aneurysm detection or extraction. As saccular aneurysms are the most common type, most studies are based on the assumption of berry-shaped aneurysms and try to identify candidate aneurysms by extracting vessel skeletons, morphological descriptors, or distance transformation. We divide the papers into two categories: image-based and surface-based. The categorization not only tells the input data type but also indicates their study purpose. Image-based methods work on either 2D or 3D images, and the goal is usually to detect any number of possible aneurysms. Surface-based methods take surface mesh reconstructed from volumetric data as input. The goal is usually to isolate an aneurysm by identifying its dome or neck, so morphological descriptors can be derived for treatment planning or risk assessment.

The detection strategies of image-based approaches can be further divided into three categories: shape-based, skeleton-based, and DL-based. Shape-based methods rely heavily on the assumption of spherical (berry-shaped) aneurysms and often use *blobness filters* (e.g. Hentschke et al., 2011; Nomura et al., 2014; Jerman et al., 2015a) to search for candidate aneurysms with a spherical shape. Blobness filters normally depend on the eigenanalysis of the Hessian matrix of an image, and multi-scale enhancement is required in order to detect aneurysms of different sizes. Some authors (Mitra and Chandra, 2013) use mathematical morphological operations to remove relatively thin vessels to detect aneurysms. Skeleton-based methods use a 3D thinning algorithm to obtain the vessel centerlines and analyze along the centerlines to find abnormal branching patterns, such as endpoints of centerlines or

short branches (Suniaga et al., 2012). DL-based methods automatically extract features from images without assuming the aneurysm geometry and can detect both saccular and fusiform aneurysms (Sichtermann et al., 2019; Yang et al., 2021). As aneurysms are small compared to the vascular structure, it is a common practice to extract candidate ROIs for further analysis. DL-based methods often sample patches from volumetric images to not only deal with class imbalance (small aneurysm versus large background) but also to reduce computational cost. The first two categories using classical feature-based methods require further post-processing (described in the next subsection) to segment the aneurysms. Some DL-based methods can serve both as detection and segmentation algorithms if the input and output sizes of the network are identical, e.g., U-Net.

The surface-based approaches can be roughly divided into three groups: dome-based, neck-based, and DL-based. Dome-based methods (e.g. Ford et al., 2009; Larrabide et al., 2010) try to isolate the aneurysm dome by identifying non-tubular regions through deformable models. In contrast, neck-based methods (e.g. Sgouritsa et al., 2010; Cárdenes et al., 2011) look for the closed geodesic curve at the boundary between the aneurysm dome and its feeding vessel given some topological criteria. Dome- and neck-based methods usually require the computation of the vessel centerline, which is an important geometric feature for morphological analysis of vasculature. A special solution is proposed by Jerman et al. (2019), who developed an algorithm to automatically position a cutting plane to segment an aneurysm. Some of the recent papers (Schneider et al., 2021; Niemann et al., 2021; Timmins et al., 2022) proposed DL-based methods using MeshCNN (Hanocka et al., 2019), which is a variant of convolutional neural network with specialized mesh convolution and pooling operations to process mesh edges. Most surface-based approaches enable the quantification of aneurysms, thereby facilitating morphological analysis. Segmentation can be considered as part of the process, but the term is seldom referred to in the literature using surface-based approaches.

### 3.3. Post-processing

Post-processing serves to refine the result of the identified aneurysms from the previous step. For the image-based approaches, many false positives are often identified because of their sphere-like shapes after image processing. Surface-based approaches are less prone to many false positives, but post-processing is required to refine the ostium. To remove false positives, common strategies include *connected component analysis* and rule-based systems or classifiers. The rules may include criteria to remove voxels touching the image boundary or not connected to vessel structure or candidates with a volume smaller than a threshold. Additionally, geometric descriptors, such as those derived from automatic decomposition into near- and far-vessel regions and axial plane computation (Neugebauer et al., 2013b), can support further refinement and improve the accuracy of detected aneurysms. With well-established post-processing, true aneurysms can be detected and segmented as ROIs for further analysis.

### 3.4. Visualization

Once the aneurysms are segmented, further visualization methods are applied for advanced analysis and exploration. Typically, not only the vessel morphology is illustrated (Lawonn et al., 2013), but also the blood flow is visualized as well, which assumes computational fluid dynamic simulations to extract the flow information. The visualization comprises tasks of depicting near-wall flow (Neugebauer et al., 2013a; Lawonn et al., 2014), the wall thickness (Glaßer et al., 2014; Lawonn et al., 2015; Meuschke et al., 2017b), but also advanced visualizations to encode simulated information on the surface mesh (Meuschke et al., 2017c, 2019a, 2021b) as well as mechanical forces acting on the vessel wall (Meuschke et al., 2017c). Comparative visualization approaches integrating morphology and blood flow indicators can assist clinicians

in treatment assessment by simplifying the exploration of complex hemodynamic data (Van Pelt et al., 2014). Besides the visualization of the surface with blood flow, analyzing the flow pattern is also an essential task for an advanced analysis (Meuschke et al., 2018c, 2019b, 2022). This also comprises the generation of animations to support the exploration of the complex flow information (Meuschke et al., 2017a; Apilla et al., 2021). Moreover, techniques have been developed to visualize blood flow in a manner that clinicians are already familiar with, such as virtual DSA representations (Prefßer et al., 2022). An overview of the most recent visualization techniques for cerebral aneurysms is available in the framework ANEULYSIS, as described by Meuschke et al. (2021a). More recently, ANEULYSIS was extended to a web-based tool, which supports collaborative aneurysm data exploration (Prefßer et al., 2023). A more general overview of the visualization of medical flow data is given in previous state-of-the-art reports (Oeltze-Jafra et al., 2019; Eulzer et al., 2022).

### 3.5. Evaluation

The performance of algorithms for aneurysm detection and segmentation is evaluated against the ground truth (GT) provided by experienced clinicians. Detection and segmentation are evaluated using different performance metrics. Even though the same metrics may be used in both tasks, the interpretation of the parameters differs. Therefore, we outline the common performance metrics for both tasks in separate subsections.

#### 3.5.1. Detection metrics

Detection algorithms can be evaluated using common metrics like accuracy, sensitivity, and the area under the receiver operating characteristic (AUC-ROC) curve either by *patient-level* (image-level) or *lesion-level* analysis. Patient-level analysis evaluates the correctly identified patients (scans) with aneurysms. Given the GT and the prediction, we can define four possible outcomes: true positive (TP), true negative (TN), false positive (FP), and false negative (FN), where positive and negative refer to a patient or a scan with or without any aneurysm. The lesion-level analysis evaluates the correctly identified aneurysms of all existing aneurysms within the datasets. In this case, the meaning of TP, FP, and FN requires the usage of the bounding box from object detection. In the CADA challenge (Ivantsits et al., 2020a), a predicted aneurysm is considered as TP if the center of its bounding box intersects with the GT aneurysm mask. An FP may indicate an aneurysm is found either around healthy vessels or away from the true location. TN is meaningless according to such a definition, and thus, specificity is undefined for lesion-level analysis. We can tell that lesion-level analysis is stricter than patient-level due to its requirement for precise localization of every individual lesion, rather than merely identifying the presence of an aneurysm in a patient or scan. Hence, these two forms of analysis are incomparable.

One of the most widely used tools for evaluating the performance of aneurysm detection is the free-response receiver operating characteristic (FROC) curve, which shows the sensitivity versus the average number of FPs per image or lesion. FROC is a variant of ROC, which illustrates the performance of a binary classifier with varying thresholds by showing the true positive rate against the false positive rate. Since FNs are not considered in the calculation, ROC is unsuitable for imbalanced data. FROC takes into account multiple pathologies and pathology localization information (Thompson, 2015). Therefore, FROC is widely used for assessing image-based aneurysm detection algorithms which can detect multiple aneurysms but may produce several FPs.

Intersection over union (IoU) is a common metric to assess the object detection performance based on the Jaccard index:

$$J(B_p, B_{gt}) = IoU = \frac{area(B_p \cap B_{gt})}{area(B_p \cup B_{gt})} \sim \frac{TP}{TP + FP + FN}. \quad (1)$$

where  $B_p$  and  $B_{gt}$  respectively denote the bounding box area of the prediction and that of the ground truth. Unlike typical object detection in natural images, aneurysm detection algorithms seldom directly predict bounding boxes, so the calculation of IoU is normally calculated by the rightmost of Eq. (1). Average precision (AP) quantifies the precision of object detection for a single class across different recall levels. AP is calculated by integrating the area under the precision-recall curve. Mean average precision (mAP) extends AP to multiple classes by taking the mean of the AP scores across all classes in the dataset. More information on object detection metrics can be found in Padilla et al. (2020).

#### 3.5.2. Segmentation metrics

The performance of segmentation algorithms is assessed based on how accurately they delineate aneurysm boundaries compared to the GT derived from manual annotations by clinicians. The prediction also has four possible outcomes, i.e., TP, TN, FP, and FN, but the prediction being positive or negative is defined on a per-pixel or per-voxel basis.

Segmentation tasks are usually assessed by the Dice similarity coefficient (DSC), IoU, mAP, and Hausdorff distance (HD). DSC is defined as follows:

$$DSC(P, G) = \frac{2|P \cap G|}{|P| + |G|} = \frac{2 \sum_i^N p_i g_i}{\sum_i^N p_i + \sum_i^N g_i} = \frac{2TP}{2TP + FP + FN}, \quad (2)$$

where  $p_i \in P$  is the predicted segmentation region,  $g_i \in G$  is the ground truth segmentation region, and  $N$  is the number of pixels or voxels. IoU also called the Jaccard index, is defined similarly but differs from that of detection (Eq. (1)):

$$IoU(P, G) = \frac{|P \cap G|}{|P \cup G|} = \frac{\sum_i^N p_i g_i}{\sum_i^N p_i + \sum_i^N g_i - \sum_i^N p_i g_i} = \frac{TP}{TP + FP + FN}. \quad (3)$$

mAP is the average precision of all categories detected, that is, the average precision of segmenting the aneurysms and the background:

$$mAP = \frac{1}{C} \sum_i^C \frac{|TP_i|}{|TP_i| + |FP_i|}, \quad (4)$$

where  $C$  is the number of classes. Hausdorff distance is the maximum distance of a set to the nearest point in the other set:

$$H(P, G) = \max(h(P, G), h(G, P)), \quad (5)$$

where

$$h(P, G) = \max_{p \in P} \min_{g \in G} \|p - g\|.$$

Unlike the previous metrics whose ideal value is 1, the optimal Hausdorff distance is 0. Due to the inherent characteristics of imaging and geometric data, the meaning of these metrics varies. Image-based evaluation is more concerned with the accurate delineation of the object in a volumetric sense, making overlap and classification metrics more relevant. On the other hand, surface-based evaluation emphasizes the precision of the contour or surface shape.

For quantitative morphological analysis, such as aneurysm height or neck width, a common tool is the Bland–Altman plot, a graphical method to visualize the agreement between two measurements (estimated morphological descriptors by human experts and by algorithms). The plot shows the difference in measurements against the average measurement. In the literature, the ostium extraction is assessed by Hausdorff distance or the average inter-curve distance (Cárdenes et al., 2013), a curve-based metric for measuring the difference between the automatically ( $\gamma_a$ ) and manually ( $\gamma_m$ ) defined ostium:

$$d_{a,m} = \left( \frac{2}{L_a + L_m} \right) \int_0^1 d(\gamma_a(s), \gamma_m(s)) ds, \quad (6)$$

with the curve length

$$L_i = \int_0^1 \|\gamma_i(s)\| ds \quad (7)$$

Here,  $s$  serves as a parametric variable standardizing the curve length from 0 to 1, facilitating a direct comparison between  $\gamma_a(s)$  and  $\gamma_m(s)$ , despite their potentially differing lengths and shapes. Other morphological parameters are scalar and can be assessed by Pearson correlation coefficient or relative error.

In the realm of aneurysm detection and segmentation, sensitivity emerges as a predominant metric due to its critical role in ensuring all true aneurysms are identified accurately. The importance of sensitivity is often highlighted in analyses employing the FROC curve, which provides sensitivity values at varying FP rates per case, enabling a nuanced evaluation of detection performance. However, the lack of universally accepted standards for evaluating aneurysm detection and segmentation poses challenges in comparing methodologies across studies. It is imperative to consider the specific objectives of the study, the characteristics of the dataset, and the level of analysis when selecting appropriate metrics. General guidelines for metrics selection in medical imaging analysis can be found in [Taha and Hanbury \(2015\)](#) and [Maier-Hein et al. \(2024\)](#).

#### 4. Taxonomy

One of the main purposes of this survey is to define a taxonomy, which categorizes the aneurysm detection and segmentation algorithms in the literature from three perspectives:

- Data: raw data (input data), number of datasets, multiplicity
- Task: objective, ostium extraction, morphological descriptors measurement
- Methodology: automaticity, strategy and features, DL-based, vessel segmentation, metrics

Through the taxonomy, we provide a comprehensive overview of the related algorithms and understand their differences and the trends and limitations in the research of CAD aneurysm detection systems. Interested readers can also refer to the papers whose data and approach correspond to their own experiment settings and designs.

##### 4.1. Data

We look at four aspects of the data: input data structure, raw data, number of datasets, and multiplicity (number of aneurysms per dataset). In [Tables 4, 5 and 6](#), the taxonomy is color-coded by the input data structure (3D surface, point sets, volumetric images, 2D images), which is associated with the methodology and the task. We consider the actual data format being processed by the algorithm as the input data structure to distinguish from raw data which can be either 2D or 3D angiography. One important observation from the table is that 3D surface data is used mostly for aneurysm quantification, ostium extraction, and measuring morphological descriptors, such as aneurysm dome height and neck width. 3D surface meshes are used since they contain more geometry information than volumetric data so that morphological descriptors can be more easily estimated. Despite several deep learning frameworks for surface data such as MeshCNN ([Hanocka et al., 2019](#)), point sets are still easier to process using an existing framework like PointNet ([Qi et al., 2017a](#)). Therefore, some recent studies (e.g., [Bizjak et al., 2020](#)) process the vertices of the 3D surface without considering the connectivity information.

The imaging modality has an impact on the preprocessing step for vasculature extraction, but as long as the parameters for processing are properly adjusted, the same aneurysm detection algorithm can work in multiple modalities ([Neugebauer et al., 2010](#); [Hernandez and Frangi, 2007](#); [Lauric et al., 2010](#); [Bogunović et al., 2011](#); [Hassan et al., 2011](#); [Hentschke et al., 2011, 2012, 2014](#); [Jerman et al., 2015b](#)). The main difference between modalities is the number of visible vessels ([Hentschke et al., 2011](#)). DSA is widely used for 2D image-based approaches because it shows higher contrast between vessels and the

background than other modalities. MRA, which is prone to several imaging artifacts, is the most commonly used modality in 3D image-based approaches, particularly for DL-based methods. The reason may be that MRA requires no contrast agents and is less invasive than other modalities, so collecting a large amount of data from both patients and healthy controls for screening is more achievable. 3DRA and MRA are more often used in the literature than CTA probably because of the public datasets from the open challenges.

The number of datasets serves two purposes: whether the algorithm of the study was validated on a variety of aneurysms, and whether the algorithm is data-driven using DL-based methods. The column “IA” (intracranial aneurysm) denotes the number of aneurysms present per dataset in the study, providing insights into the study design. For example, “0-” signifies studies containing datasets without and with aneurysms of various multiplicities. The asterisk in the superscript indicates whether fusiform aneurysms are included in the study. While primarily reflecting the study design, the column may indirectly convey the capability of the algorithm to detect multiple aneurysms within a single dataset. Notably, some image-based studies may exclude negative cases, shedding light on study design rather than the algorithm’s inability to differentiate between healthy and diseased vasculature. A major limitation of early surface-based approaches is that they locate only one aneurysm even if the vasculature is healthy or has multiple aneurysms ([Ford et al., 2009](#); [Cárdenes et al., 2011](#); [Bruijns, 2003](#); [Mohamed et al., 2010](#)).

##### 4.2. Task

Regarding the task, we are interested in the objective of an algorithm. Usually, the aim is to detect and localize unknown aneurysms in the brain or to accurately segment or quantify the volume of the aneurysms. Quantification is essential for the treatment decision, allowing the assessment of the shape and size of the aneurysms associated with the rupture risk ([Ivantsits et al., 2020b](#)). Therefore, most algorithms for aneurysm quantification also extract the ostium or morphological descriptors. In many studies using surface-based approaches, the actual objective is a morphological analysis that requires the quantification of aneurysms.

##### 4.3. Methodology

We select five aspects of the methodology for categorization: automaticity, strategy, features, DL (whether the method is DL-based), and vessel segmentation (whether vessel segmentation is required). *Automaticity* refers to whether an algorithm is free from user interaction to detect or segment aneurysms, such as point selection on the aneurysm sac ([Ford et al., 2009](#)). All the papers we selected are either semi-automated or fully automated. There are some papers whose proposed method requires manual vessel segmentation or surface reconstruction ([Yang et al., 2020b](#)) as a prerequisite, but we still consider them as automated, as the manual process is not during the aneurysm detection. We found that most available methods are automated, except for a few ones that use classical image analysis techniques, e.g. cutting plane ([Ma et al., 2004](#)), level set ([Nikravanshalmani et al., 2010](#); [Firouzian et al., 2011](#)). The *strategy* includes the main algorithms and methods for aneurysm detection. For DL-based approaches, the strategy refers to the network architecture. Non-DL-based approaches often require multiple methods to identify shape descriptors, aneurysm candidates, and FP removal. There are cases in which the approach contains several steps and algorithms, so we chose to summarize them with the most relevant step or strategy. The *feature* column lists the deciding manually extracted features for aneurysm detection, such as centerline and curvature. For approaches with rule-based systems for FP removal, we chose a general term (e.g. shape, spatial) to group and summarize different features. As DL-based approaches automatically extract features, we leave the corresponding cells in the table empty.

**Table 4**

Summary of the reviewed literature using geometric data as input. The taxonomy categorizes the studies from four perspectives: data, task, methodology and metrics. The papers are ordered by raw data and chronologically. “#Datasets” shows the number of datasets for each modality, with “/” separating the training and test data and “<sup>m</sup>” denoting multi-center study. “IA” denotes the number of aneurysms present per dataset, with “\*” indicating fusiform ones. Abbreviations are used: Morph: morphological analysis, Auto: automated method, DL: deep learning-based, Ves: vessel segmentation required. The descriptions of the studies using surface-based and point-based data are in Sections 5.1 and 5.2, respectively.

References	Data			Task			Methodology			Metrics	
	Raw data	#Datasets	IA	Objective	Ostium	Morph	Auto	Strategy; Features	DL	Ves	Sensitivity/FPs; DSC <sup>d</sup>
<b>3D surface</b>											
Wong and Chung (2006)	3DRA	17	*0-	Abnormality detection			Surface matching; centerline			✓	
Ford et al. (2009)	3DRA	10	1	Aneurysm removal			Voronoi; centerline				
Larrabide et al. (2010)	3DRA	10	1	Quantification			Deformable model; centerline, skeleton			✓	
Larrabide et al. (2011)	3DRA	26	1	Quantification			Deformable model; centerline, skeleton			✓	
Mohamed et al. (2010)	3DRA	19	1	Geometry analysis			Deformable model; centerline, curvature			✓	
Sgouritsa et al. (2010)	3DRA	19	1	Geometry analysis			Minimum s-t cut; centerline, curvature			✓	
Piccinelli et al. (2012)	3DRA	10	1	Geometry analysis			Voronoi; centerline			✓	
Saalfeld et al. (2018)	3DRA	100	1	Geometry analysis			Distance analysis, ray casting; centerline, angles			✓	
Felde et al. (2021)	3DRA	159/35 <sup>m</sup>	1-	Segmentation			Graph cut, SVM; curvature			✓	
Meuschke et al. (2018b)	3DRA	10	1	Geometry analysis			Dijkstra, geodesics; curvature, skeleton			✓	
Schneider et al. (2021)	3DRA	94	0-1	Segmentation			MeshCNN; edge parameters			✓	
Ma et al. (2004)	CTA	5	1	Geometry analysis			Cutting plane;			✓	
Prasetya et al. (2011)	CTA			Detection			Curvature analysis; curvature			✓	
Chowriappa et al. (2013)	CTA	10		Vascular decomposition			Convex decomposition, SVM; curvature, spectrum			✓	
Kohout et al. (2013)	CTA		1	Neck identification			Probability map; centerline			✓	
McLaughlin and Noble (2002)	3DRA, MRA	4	1	Quantification			Region splitting; radius			✓	
Neugebauer et al. (2010)	CTA, MRA	7	1	Ostium extraction			Geodesics; centerline			✓	
Lawonn et al. (2019)	3DRA, MRA	50, 1	1-	Segmentation			Graph cut, KNN; curvature			✓	
Zhou et al. (2019a)	3DRA, MRA	56, 65 <sup>m</sup>	0-1	Detection			GoLeNet Inception v3; multiview			✓	
Zhou et al. (2019b)	3DRA, MRA	56, 50 <sup>m</sup>	0-1	Detection			GoLeNet Inception v3; curvature, shape distance function, wave kernel signature			✓	
Timmins et al. (2022)	CTA, MRA	10, 103	0-	Segmentation			MeshCNN; edge parameters			✓	
Jerman et al. (2019)	3DRA, CTA, MRA	5, 45, 5 <sup>m</sup>	1	Quantification			Cutting plane; centerline			✓	
<b>Point sets</b>											
Yang et al. (2020b)	MRA	103	1-	Segmentation			PointNet++, SO-Net; points			✓	
Yu et al. (2021)	MRA	103	0-	Segmentation			Point transformer; normals			✓	
Shao et al. (2022)	MRA	103	0-	Segmentation			Contrastive learning, PointNet, PointNet++; point pose			✓	
Yang et al. (2023)	MRA	103	*1-	Segmentation			PointNet++, SO-Net; points			✓	
Cao et al. (2024a)	MRA	116	0-	Segmentation			Dual-branch network; spatial/pixel			✓	
Bizjak et al. (2020)	3DRA, CTA, MRA	57, 28, 5	0-	Segmentation			MLP; points			✓	
Bizjak et al. (2021)	3DRA, CTA, MRA	57, 5, 5	0-	Detection			PointNet; points			✓	
Bizjak et al. (2022)	CTA, MRA	300, 200	0-	Detection			PointNet; points			✓	

**Table 5**

Summary of the reviewed literature (continued): volumetric data. The studies using classical image processing approaches and DL-based methods are respectively described in Sections 6.1 and 6.2.

References	Data			Task			Methodology			Metrics	
	Raw data	#Datasets	IA	Objective	Ostium	Morph	Auto	Strategy; Features	DL	Ves	Sensitivity/FPs; DSC <sup>d</sup>
<b>Volumetric data</b>											
Bruijns (2003)	3DRA	4	1	Quantification			✓	Manhattan distance transform; distance		✓	
Karmonik et al. (2004)	3DRA	2	1	Geometry analysis	✓	✓	✓	Cross section analysis; vessel center		✓	
Bruijns (2005)	3DRA	28	1	Quantification			✓	Ray casting, distance thresholding; distance		✓	
Bruijns et al. (2007)	3DRA	51	1	Neck correction	✓		✓	Rule-based tubular model; shape information		✓	
Cárdenes et al. (2011)	3DRA	26	1	Neck detection	✓	✓	✓	Voronoi, fast marching; centerline, distance		✓	
Jerman et al. (2015b)	3DRA	25	1-	Quantification, geometric analysis	✓	✓	✓	Random decision forest, ray-casting, RANSAC; centerline, spherical harmonics			
Jerman et al. (2017)	3DRA	15	1-	Detection			✓	2D CNN; intra-vascular distance		✓	
Hu et al. (2020)	3DRA	145	1-	Detection			✓	Bayesian-optimized filter;			0.964
Ivantsits et al. (2020b)	3DRA	109/22	0-	Detection			✓	3D U-Net;	✓	✓	0.866/0.41
Jia et al. (2020)	3DRA	109/22	0-	Detection			✓	3D attention U-Net, RF; skeleton, radiomics	✓	✓	
Ma and Nie (2020)	3DRA	109/22	0-	Segmentation			✓	3D nnU-Net;		✓	0.886 <sup>d</sup>
Shit et al. (2020)	3DRA	109/22	0-	Segmentation			✓	Av-Net;		✓	0.682 <sup>d</sup>
Su et al. (2020)	3DRA	109/22	0-	Segmentation			✓	3D attention U-Net;		✓	0.907 <sup>d</sup>
Liu et al. (2021)	3DRA	388/63	1-	Detection			✓	3D U-Net;		✓	0.986/1.49
Li et al. (2022)	3DRA	109	0-	Segmentation			✓	2D U-Net with transformer; gradient entropy		✓	0.944 <sup>d</sup>
Lin et al. (2023)	3DRA	223, 109 <sup>m</sup>	0-	Segmentation			✓	3D U-Net++ with custom blocks;		✓	0.874 <sup>d</sup>
Nikravanshalmani et al. (2010)	CTA	15	0-	Segmentation				Level set; edges		✓	
Nikravanshalmani et al. (2013)	CTA	15		Segmentation				Conditional morphology segmentation, level set; edges		✓	
Chen et al. (2014)	CTA	8?	1	Segmentation			✓	Lattice Boltzmann, geodesic active contour; edges			
Park et al. (2019)	CTA	703/115	0-	Segmentation			✓	HeadXNet;		✓	0.949 <sup>p</sup> /0.165
Shahzad et al. (2020)	CTA	253	1-	Segmentation			✓	DeepMedic;	✓	✓	0.82/0.81, 0.75 <sup>d</sup>
Shi et al. (2020)	CTA	1177/211 <sup>m</sup>	0-	Segmentation			✓	DA-ResUNet;		✓	0.846 <sup>p</sup> /0.27; 0.53 <sup>d</sup>
Bo et al. (2021)	CTA	1338/138 <sup>m</sup>	0-	Segmentation			✓	GLIA-Net;		✓	0.720/2.72; 0.768 <sup>d</sup>
Ma et al. (2021)	CTA	145	1-	Segmentation			✓	Faster R-CNN, V-Net; image with 3D information projection		✓	0.960/1.933, 0.471 <sup>d</sup>
Meng et al. (2021)	CTA	100	1-	Segmentation			✓	Parallel CNN;		✓	0.705 <sup>d</sup>
Yang et al. (2021)	CTA	1068/400 <sup>m</sup>	*0-	Detection			✓	ResNet-18 with attention;		✓	0.975/13.8
Wu et al. (2022)	CTA	1205/303 <sup>m</sup>	1-	Rupture prediction			✓	FPN, ResNet, V-Net;	✓	✓	0.9/1
Zhu et al. (2022)	CTA	101	1-	Segmentation			✓	U-Net, V-Net, Res-UNet;		✓	0.818 <sup>d</sup>
Wang et al. (2023)	CTA	1249/134	*1-	Detection			✓	3D DAResUNet;		✓	0.97 <sup>p</sup> /0.649
Cao et al. (2024b)	CTA	70	1-	Segmentation			✓	semi-supervised; contextual		✓	0.824/0.627
Hu et al. (2024)	CTA	16546	0-	Detection			✓	Global context network, local fine-grained network;		✓	0.957 <sup>p</sup>
Arimura et al. (2004)	MRA	60	*0-	Detection			✓	Hessian-based filter, rule-based; gray-level, geometric features, skeleton			1/2.4
Arimura et al. (2006)	MRA	115/63 <sup>m</sup>	0-	Detection			✓	Hessian-based filter, rule-based; gray-level, geometric features, skeleton		✓	0.97/3.8

(continued on next page)

#### 4.4. Metrics

We specifically look at the most commonly reported performance metrics for aneurysm detection and segmentation in the literature, i.e. sensitivity and Dice similarity coefficient (DSC). The letter “d” in superscript indicates that the value is DSC. For volumetric data, the

superscript “p” means the patient-level assessment.

#### 5. Approaches with 3D geometric data

This section summarizes approaches using 3D geometric data, including surface meshes and point sets for aneurysm detection and

**Table 5 (continued).**

References	Data	Task			Methodology				Metrics			
		Raw data	#Datasets	IA	Objective	Ostium	Morph	Auto	Strategy; Features	DL	Ves	Sensitivity/FPs; DSC <sup>d</sup>
Kobashi et al. (2006)	MRA	16	*1-	Detection				✓	Case-based reasoning; radius, intensity and geometric features	✓		1/6.438
Uchiyama et al. (2006)	MRA	20	0–1	Detection				✓	Gradient concentrate filter; intensity and geometric features	✓		1/1.85
Yang et al. (2011)	MRA	287	*0-	Detection				✓	Hessian-based filter, geometry analysis; centerline, radius, curvature	(✓)	0.96 <sup>a</sup> /11.6	
Suniaga et al. (2012)	MRA	20	1	Detection				✓	Hessian-based filter, SVM; centerline, intensity, geometric features	✓		1/3.86
Nomura et al. (2014)	MRA	490/1779	0–1	Detection				✓	Hessian-based filter, CCA, boosting; shape, spatial features	✓		89.5/3
Hanaoka et al. (2015)	MRA	300		Detection				✓	Graph, SVM, CCA; HoTPiG	✓		81.8/3
Jin et al. (2016)	MRA	30	1-	Detection				✓	Ellipsoid convex enhancement filter;			1/31.8
Nakao et al. (2018)	MRA	350/100	1-	Detection				✓	2D CNN; concatenated MIP	✓	✓	0.942/2.9
Sichtermann et al. (2019)	MRA	68/17 <sup>m</sup>	*1-	Detection, segmentation				✓	DeepMedic;	✓		0.9/6.1; 0.53 <sup>d</sup>
Ueda et al. (2019)	MRA	683/588 <sup>m</sup>	1-	Detection				✓	ResNet18;	✓		0.925/5
Baumgartner et al. (2020)	MRA	113	0-	Detection				✓	3D Retina U-Net;	✓		
Chen et al. (2020)	MRA	76/55 <sup>m</sup>	1-	Detection				✓	3D U-Net;	✓	✓	0.829/0.86
Faron et al. (2020)	MRA	85 <sup>m</sup>	1-	Detection				✓	DeepMedic;	✓		0.90/6.1
Hou et al. (2020)	MRA	164 <sup>m</sup>	1-	Detection				✓	1D CNN; vectors from MIP	✓	✓	0.932
Joo et al. (2020)	MRA	468/226 <sup>m</sup>	0-	Detection				✓	ResNet;	✓	✓	0.857
Shimada et al. (2020)	MRA	1623		Detection				✓	ResNet-18;	✓		
Assis et al. (2021)	MRA	100/11	1-	Detection				✓	3D U-Net;	✓		0.830/0.44
Di Noto et al. (2022)	MRA	397 <sup>m</sup>	0-	Detection				✓	3D U-Net; ROIs at 20 landmark points	✓		0.83/0.8
Ye et al. (2022)	MRA	143/177 <sup>m</sup>	0-	Segmentation				✓	OTO-Net;	✓		0.972 <sup>d</sup>
Yuan et al. (2022)	MRA	489 <sup>m</sup>	0-	Segmentation				✓	DCAU-Net;	✓		0.788; 0.746 <sup>d</sup>
Zhou and Huang (2022)	MRA	113	0-	Segmentation				✓	IntrAsegTran (transformer);	✓		0.919 <sup>a</sup> /0.10; 0.58 <sup>d</sup>
Assis et al. (2023)	MRA	402 <sup>m</sup>	1-	Detection, pose estimation				✓	ResNet;	✓		0.830/0.44
Claux et al. (2023)	MRA	24/25	1-	Detection				✓	3D U-Net;	✓		0.78/0.5
Ham et al. (2023)	MRA	120/132 <sup>m</sup>	1-	Detection, segmentation				✓	3D U-Net;	✓	✓	0.879; 0.682 <sup>d</sup>
Lauric et al. (2010)	3DRA, CTA	10, 10	0-	Detection				✓	Shape analysis; skeleton, writh number	✓		1/0.66, 1/5.36
Hassan et al. (2011)	CTA, MRA	15, 5		Quantification, localization				✓	Diameter variation analysis; centerline	✓		
Hentschke et al. (2011)	3DRA, CTA, MRA	30, 15, 20	0-	Detection				✓	Hessian-based filter, k-means, rule-based; intensity, shape, spatial features			0.963/2.6, 0.895/20.8, 0.938/8.0
Hentschke et al. (2012)	CTA, CE-MRA, TOF-MRA	34, 12, 20	0-	Detection				✓	Hessian-based filter, CCA, rule-based; intensity, shape, spatial features			0.963/20.9, 1/8.75, 0.93/11.3
Hentschke et al. (2014)	CTA, CE-MRA, TOF-MRA	72, 69, 10	*0-	Detection				✓	Hessian-based filter, CCA, linear discriminant function; intensity, shape, spatial			0.95/22.8, 0.95/8.2, 0.95/11.3
Jerman et al. (2015a)	DSA, CTA, MRA	30, 10, 2	1-	Segmentation				✓	Hessian-based filter;			

segmentation. 3D geometric data is instrumental in capturing the intricate geometric details of vascular structures, facilitating both aneurysm identification and morphological analysis. The surface mesh is especially suitable for representing smooth vascular structures, so it is the most common data format for aneurysm morphological analysis, as can be seen in Table 4. Point sets are popular for applications in which data are acquired from moving cameras for 3D scene reconstruction, such as robotics, photogrammetry, autonomous driving, and laparoscopy in the medical field (Maier-Hein et al., 2013). In recent years, some researchers illustrated the efficacy of aneurysm segmentation using point-based deep neural networks, though detailed morphological analysis is still predominantly conducted using surface data.

### 5.1. Surface mesh approaches

Many surface-based approaches aim to conduct morphological analysis of the vasculature for rupture risk assessment (Saalfeld et al., 2018; Meuschke et al., 2018b) or endovascular treatment planning (Mohamed et al., 2010; Wong and Chung, 2006). Central to these approaches are the extraction of the vessel centerline and the identification of the ostium or the neck of the aneurysm. The centerline can be obtained by thinning methods, distance transformations, or Voronoi diagrams (Neugebauer et al., 2010). The skeleton is similar to the centerline but also has branches for saccular aneurysms. Aneurysm quantification and morphological analysis require the detection of the ostium.

**Table 6**

Summary of the reviewed literature (continued): 2D images. The studies using classical image processing approaches and DL-based methods are respectively described in Sections 7.1 and 7.2.

References	Data			Task			Methodology			Metrics	
	Raw data	#Datasets	IA	Objective	Ostium	Morph	Auto	Strategy; Features	DL	Ves	Sensitivity/FPs; DSC <sup>d</sup>
<b>2D images</b>											
Dai et al. (2020)	CTA	208/103 <sup>m</sup>	1-	Detection			✓	Faster RCNN, nearby projection;	✓		0.918
Zakaria et al. (2011)	DSA		1	Detection			✓	Parameter visualization; time to peak, time duration		✓	
Mitra et al. (2013)	DSA	12	1-	Detection			✓	Hough transform, peak trekking; parameters from Hough hierarchy		✓	1
Mitra and Chandra (2013)	DSA	3	1	Detection			✓	Spatial filtering and thresholding;		✓	
Mondal and Chandra (2014)	DSA	3	1-	Detection			✓	Morphological operation, Sobel operator; intensity features		✓	0.99
Rahmany and Khlifa (2014)	DSA	2	1	Detection			✓	Fuzzy morphology;		✓	
Sulayman et al. (2016)	DSA	19	1	Detection				Morphological operation, rule-based; shape features		✓	0.895
Chandra and Mondal (2017)	DSA	15	1-	Detection			✓	Thresholding, morphological operation, Sobel operator; intensity features		✓	0.982
Malik et al. (2018)	DSA	59	0-1	Detection, rupture prediction			✓	✓	✓	✓	0.97
Rahmany and Khlifa (2018)	DSA	30	1	Detection			✓	Fuzzy logic, morphological operation; intensity features		✓	1
Rahmany et al. (2018a)	DSA	30	1	Detection			✓	Feature matching; MSER, SURF, SIFT		✓	1
Rahmany et al. (2018b)	DSA	20/10	1	Detection			✓	Inception v3;	✓		
Duan et al. (2019)	DSA	241/40	0-	Detection			✓	FPN, grayscale suppression; intensity features	✓		0.960
Rahmany et al. (2019)	DSA	20/10	*1	Detection			✓	KNN; local binary patterns, generic Fourier descriptors			0.91
Hainc et al. (2020)	DSA	565/141	0-	Detection			✓	DL software: Cognex;	✓		0.79
Podgorsak et al. (2020)	DSA	250/100	0-	Segmentation			✓	CNN;	✓		0.903 <sup>d</sup>
Zafar et al. (2021)	DSA	209	*0-1	Detection, location classification			✓	KNN; shape, texture features		✓	
Jin et al. (2019)	DSA-t	347/146	1-	Detection, segmentation			✓	FCN, BDC-LSTM;	✓		0.893/3.77, 0.533 <sup>d</sup>
Liao et al. (2019)	DSA-t	270	0-	Detection			✓	FPN, BDC-LSTM;	✓		0.880
Zeng et al. (2019)	DSA-t	300	0-	Detection			✓	VGG16; spatial information	✓		0.994
Rauf et al. (2019)	MRI	3		Segmentation			✓	Thresholding, morphological operation;			
Stember et al. (2019)	MRA	250/86	1-	Aneurysm measurement			✓	U-Net;	✓		0.988
Kashyap et al. (2022)	MRA	144	1-	Segmentation			✓	U-Net, EfficientNet;	✓		0.9 <sup>d</sup>
Anjum et al. (2018)	DSA, MRA	126, 54		Detection, rupture prediction			✓	MLP, watershed, distance transform; Haralick texture features	✓	✓	

### 5.1.1. Aneurysm isolation by tubular model

Several studies rely on centerline extraction for aneurysm detection or quantification by approximating normal vessels as tubular models. Wong and Chung (2006) reconstructed normal vasculature with cylindrical surface models to identify abnormalities, requiring manual selection of centerline endpoints in disease-free vessel sections. The abnormal vascular structures, including both saccular and fusiform aneurysms and stenosis, are then determined as the complement of

the approximated normal vessels. The work's limitations include the vessel width assumption (vessel widths change linearly along the vessel centerline) and insensitivity to flat aneurysmal sacs and mild segmental dilation. Ford et al. (2009) aimed to digitally remove aneurysms for aneurysm and post-treatment hemodynamic analysis using centerlines extracted from Voronoi diagrams, requiring a user-selected point on the aneurysm. The algorithm reconstructs the vessels guided by cubic spline interpolations, and the ostium may not be well defined.

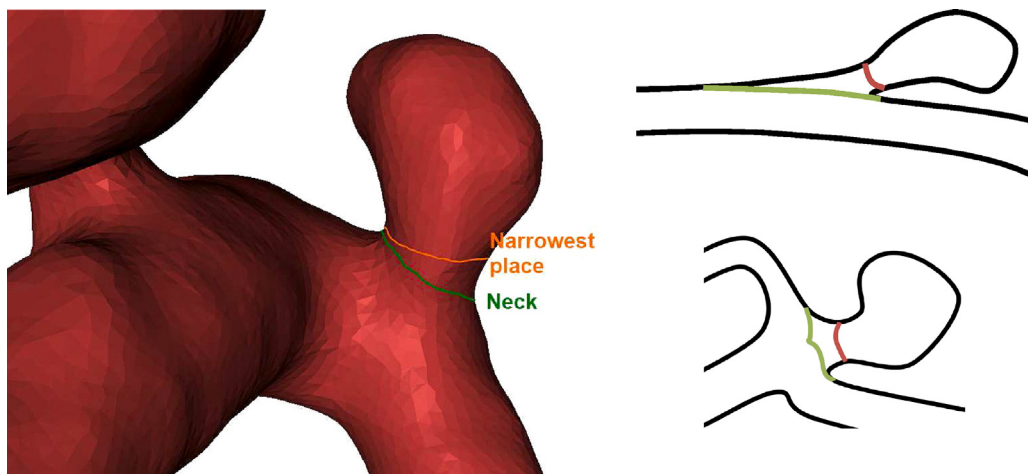


**Fig. 5.** The aneurysm neck (ostium), which divides the aneurysm from the non-pathological parent vessel, may differ from the narrowest curve.  
Source: Image from Kohout et al. (2013).

Piccinelli et al. (2012) followed Ford et al. (2009) to extract an aneurysm sac by constructing the parent vessel morphology. The authors used closed iso-surfaces along the aneurysm sac for precise neck identification through distance analysis, assuming that the neck is the contour with a minimum area. Larrabide et al. (2011, 2010) developed an automatic framework for morphological analysis of saccular intracranial aneurysms, using topology analysis to identify possible branches and deformable models to identify the neck. For vascular regions with more than one aneurysm, the skeleton processing needs to be repeated to obtain a different aneurysm branch.

#### 5.1.2. Ostium extraction

Following the initial construction of tubular models along vessels to delineate aneurysm boundaries (Larrabide et al., 2011, 2010; Piccinelli et al., 2012), some studies directly detect the neck plane (Jerman et al., 2019) or extract the ostium curve (Neugebauer et al., 2010; Ma et al., 2004; Saalfeld et al., 2018; Meuschke et al., 2018b) for quantitative aneurysm analysis. Using a cutting plane is a fast strategy to isolate an aneurysm, but it is commonly done manually (Bogunović et al., 2011). In an early work, the aneurysms are isolated by manually placing a cutting plane, and the neck curve is smoothed to eliminate sharp corners using a non-shrinking curve and surface-smoothing algorithm (Ma et al., 2004). Jerman et al. (2019) proposed an automated approach for placing a cutting plane to quantify aneurysms based on detecting specific geometric features. They first extract the parent vessel centerline of an aneurysm, localize the aneurysms, and identify the principal orientation of the sac. The cutting plane is placed by optimization using incursion, distance from the parent vessel, and curve length. Issues with the approach include the time-consuming optimization (around 20 min) and the fact that the cutting plane is unsuitable for small or flat aneurysms with low curvature.

The ostium curve can be used to better characterize the aneurysm than a neck plane, as the boundary between the aneurysm and the healthy vessel does not lie on a plane (Jerman et al., 2019). Ostium extraction requires more detailed geometric analysis, as the ostium is not necessarily the narrowest place between the aneurysm and the parent vessel (Fig. 5), and is only loosely correlated with the curvature of the surface (Kohout et al., 2013). Neugebauer et al. (2010) pioneered direct ostium reconstruction for saccular aneurysms using the centerline and a manually selected point on the aneurysm sac to define the ostium through four points based on geodesic distance. Two points are located where the aneurysm emerges from the parent vessel and the other two describe how the ostium bends around the parent vessel (Fig. 6). The definition of the points was derived from an informal study with domain experts. This method laid the groundwork of Meuschke

et al. (2018b), who automated the ostium extraction by leveraging vessel skeleton and shape index to define the ostium without manual input. The approach improved upon the previous method (Neugebauer et al., 2010) in terms of the measured morphological descriptors and the ability to handle wide neck aneurysms and small arteries around the ostium. Moreover, the authors provided a user interaction function to manually correct the identified ostium, which is useful for computer-assisted diagnosis. One common limitation of both studies is the inability to process multiple aneurysms.

Kohout et al. (2013) presented a semi-automatic method for identifying the aneurysm neck. Instead of detecting landmark points, the method is based on the probabilistic evaluation of the mutual location of surface points on the blood vessel and the skeleton of the blood vessel. The user must select the point that splits the aneurysm from the parent vessel. For complex cases in which the aneurysm is multilobular, manual editing is necessary to correct the wrong skeleton branching.

#### 5.1.3. Shape descriptor strategy

Besides the centerline and skeleton, there are some shape descriptors for detecting bulging aneurysms along the vasculature. One of the earliest studies (McLaughlin and Noble, 2002) defined the vessel radius and perpendicular width as shape descriptors over a surface mesh and used a novel region-splitting algorithm termed seed and cull algorithm to identify the section of the mesh covering the aneurysm. Curvature, particularly Gaussian curvature (Mohamed et al., 2010) and shape index (Prasetya et al., 2011; Lawonn et al., 2019; Felde et al., 2021), emerged as a critical feature for saccular aneurysm detection. Gaussian curvature (do Carmo, 1976) is the product of the two principal curvatures  $\kappa_1, \kappa_2$ , while the shape index (Koenderink and Van Doorn, 1992) is defined as:

$$S = \frac{1}{2} - \frac{1}{\pi} \operatorname{atan} \left( \frac{\kappa_1 + \kappa_2}{\kappa_1 - \kappa_2} \right). \quad (8)$$

Gaussian curvature and shape index are more robust than curvature. This is particularly true for the shape index, which is based on the ratio of the principal curvatures and is therefore invariant to scaling. Fig. 7 displays a saccular aneurysm color-coded by the value of Gaussian curvature.

Mohamed et al. (2010) used a deformable contour model based on Gaussian curvature and a distance measure to localize the aneurysm neck and separate its dome surface from the neighboring vessels. The morphological descriptors (neck length, dome height, and maximum diameter of the aneurysm) are estimated after approximating the aneurysmal neck by an ellipse. The major limitation is that the method

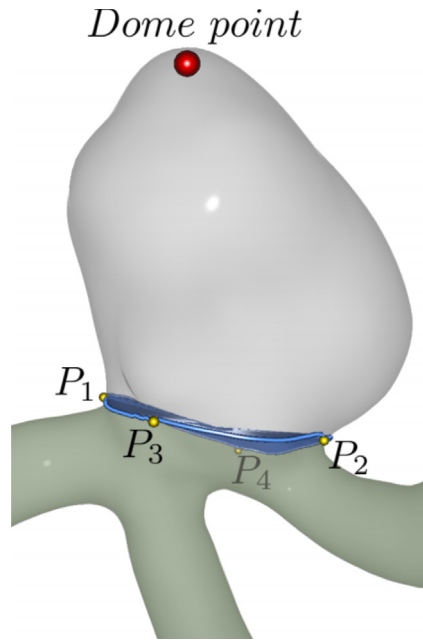


**Fig. 6.** The ostium is extracted by four landmarks. Two points  $P_1, P_2$  are located where the aneurysm emerges from the parent vessel, and the other two  $P_3, P_4$  are on the bent geodesic curve around the parent vessel.

Source: Image from Meuschke et al. (2018b).

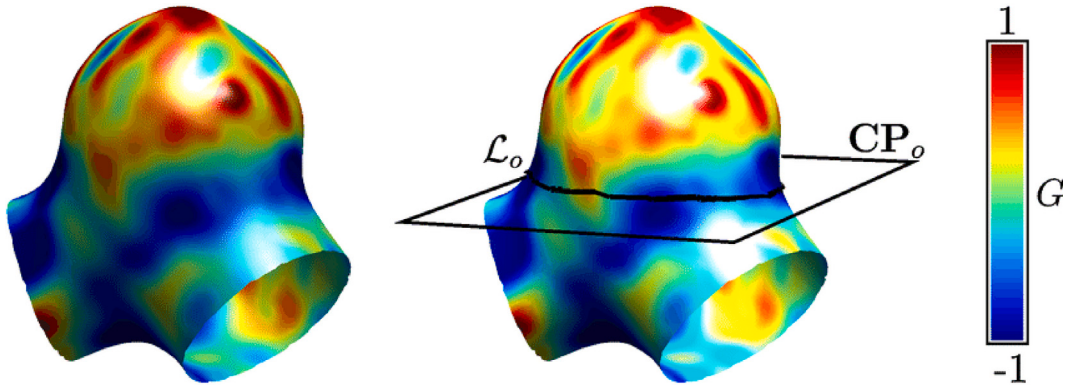


**Fig. 7.** Color-coded values of the Gaussian curvature are computed on the vascular surface mesh.  
Source: Image from Jerman et al. (2016).

can reach a local minimum. Sgouritsa et al. (2010) proposed a graph-based approach by considering aneurysm segmentation as a minimum s-t cut problem. The costs of the edges in the graph are assigned in such a way that the minimum cut consists of edges of high curvature around the aneurysm neck. The method guarantees a globally optimal solution while restricting the set of feasible solutions for the neck to single closed contours.

Chowriappa et al. (2013) considered vascular decomposition as a cluster optimization problem, which allows for aneurysm and vessel segmentation. They first construct a dual graph from the vasculature mesh weighted by the shape index and apply convex decomposition (mesh decimation) to separate the vasculature into a geometrically consistent set of regions. Vessel classification is performed on the decomposed regions using a support vector machine (SVM) based on the Laplacian spectrum. As spectral shape descriptors, the Laplacian eigenvalues can be considered as mesh frequencies, whose corresponding low-frequency eigenvectors capture the global shape characteristics. By taking the  $k$  smallest eigenvalues, the vascular manifold is embedded into a  $k$  dimensional subspace spanned by their associated eigenvectors.

The authors found that  $k = 11$  was optimal to distinguish between aneurysms and non-pathological vessels. An overview of the spectral approach is illustrated in Fig. 8.

Lawonn et al. (2019) developed a three-stage geometric optimization method for identifying multiple aneurysms. In the first stage, candidate regions are identified by global optimization and graph cut based on shape index and the heuristics that aneurysms are spherical while the border between an aneurysm and the vessel is rather saddle-like. A smoothing parameter helps to regularize the process by encouraging neighboring triangles to have the same label. The second stage uses four shape-based features to remove false positives through a weighted k-nearest neighbor classifier. The third stage allows the user to correct the segmentation via a brushing interface, with the ostium curve refined via an anisotropic diffusion scheme. Felde et al. (2021) modified the approach of Lawonn et al. (2019) to detect and segment aneurysms for numerical fluid analysis. They applied graph cuts using a surface shape index with connected component analysis to identify candidate aneurysm triangles on the surface mesh and refine the segmented regions through iterative optimization. The final

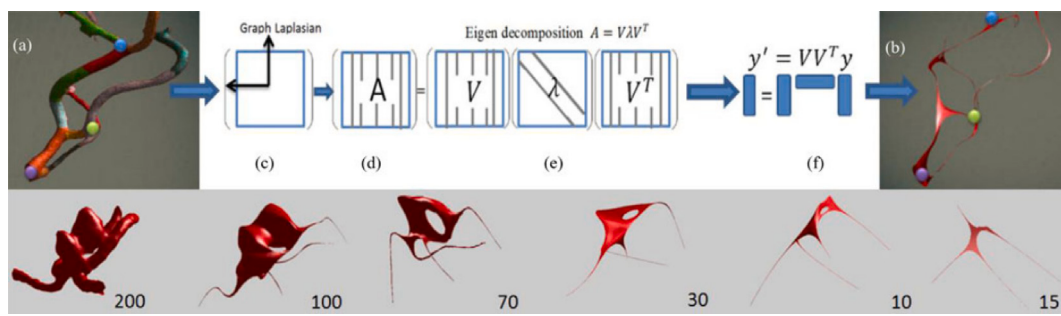


**Fig. 8.** An overview of the spectral embedding process for aneurysm detection. The vascular surface (a) can be embedded in a subspace (b) spanned by the first  $k$  eigenvectors obtained by eigenanalysis (c)–(f). The bottom shows the embedded vessel with an aneurysm using varying numbers (200 to 15) of eigenvectors.  
Source: Image from Chowriappa et al. (2013).

candidates are classified using an SVM with shape index and diffusion features.

#### 5.1.4. DL-based methods

Deep neural networks were utilized to process mesh data for aneurysm detection (Zhou et al., 2019a,b) and segmentation (Schneider et al., 2021; Timmins et al., 2022). To process unordered and irregular mesh data, either the operations of the networks need to be modified or the data needs to be transformed. Schneider et al. (2021) and Timmins et al. (2022) made use of the edge-based convolutional neural networks (CNN) called MeshCNN (Hanocka et al., 2019) to segment aneurysms. Five geometric features (the dihedral angle, two inner angles, and two edge-length ratios), which are scale-, translation-, and rotation-invariant, are extracted from each edge as the input for the tailored convolutions and pooling based on the 1-ring edge neighborhood. Schneider et al. (2021) tried to segment vascular structures into four classes (vessel, aneurysm, inlet, bifurcation) and achieved an IoU of 71.4% for the aneurysm class. Timmins et al. (2022) validated their performance in vessel meshes from both MRA and CTA and reported a lower false positive rate in MRA.

Zhou et al. (2019a) tackled mesh processing through data transformation, employing multi-view images generated from surface models using the Phong reflection model. They used PCA to determine view directions and optimized the number of views to nine, balancing shape visibility and occlusion. Furthermore, they introduced a transferable multi-model ensemble (MMEN) architecture for enhanced detection, using conformal mapping of local and global spectral descriptors to train pre-trained GoogleNet Inception v3 models. A detection accuracy of 95.1% was achieved, but the validation was limited to bifurcations on the anterior cerebral artery (ACA) and internal carotid artery (ICA).

#### 5.2. Point sets approaches

With the advance of deep learning in medical data analysis, the processing of surface data remains a challenge. Despite using the edge-based DL framework MeshCNN in some studies (Schneider et al., 2021; Timmins et al., 2022), the DL-based segmentation methods for surface mesh are still limited and were not specifically designed for medical data. Point sets (point clouds) provide an alternative way to maintain useful geometric information while allowing the use of more well-established deep learning algorithms, such as PointNet (Qi et al., 2017a), PointNet++ (Qi et al., 2017b), and So-Net (Li et al., 2018). 3D points still require the reconstruction of surface models from volumetric data since they are commonly taken from the vertices of the 3D surface, but the aneurysm detection methods for point sets are modality-independent if the surface models are properly reconstructed.

Bizjak et al. (2020) proposed an aneurysm segmentation based on point cloud data. Given the extracted vasculature, they applied surface mesh parcellation to highlight aneurysm regions and employed PointNet for point classification within these areas (Bizjak et al., 2021,

2022).

Yang et al. (2020b) created a pipeline also for aneurysm segmentation. Artery fragments are first randomly sampled and are classified by PointNet++ to predict the existence of aneurysms. The pathological fragments are passed to the SO-Net for aneurysm segmentation, achieving an average DSC of 0.718. Shao et al. (2022) also presented a classification-segmentation pipeline with a self-supervised learning framework (Fig. 9). The point clouds first undergo contrastive learning via the dual-branch encoders, a PointNet and a PointNet++, which respectively extract global and local features to distinguish between features of healthy and aneurysmal vessels. The concatenated features from the encoders are passed to linear/1D convolutional layers for classification/segmentation.

Incorporating point-based transformers (Guo et al., 2021; Zhao et al., 2021; Yuan et al., 2022) presented the 3D medical point transformer (3DMedPT) for point cloud analysis, leveraging attention mechanisms to dynamically adjust focus on relevant input segments. Transformers were originally proposed for natural language processing (Vaswani et al., 2017) to process long sequences. The core component of transformers is the self-attention module, which assigns the relevance of the elements within an input sequence with respect to the overall context. It is invariant to the permutation and cardinality of the input elements. These properties are suitable for the analysis of unordered points. The authors apply position embeddings to learn accurate local geometry and multi-graph reasoning (MGR) to examine global knowledge propagation over channel graphs to enrich feature representations. The efficiency of 3DMedPT was demonstrated by comparing it with other point-based networks in aneurysm classification and segmentation using the IntrA dataset (Yang et al., 2020a), reaching a DSC of 0.897 in segmentation.

#### 5.3. Summary of geometric data approaches

In summary, surface mesh and point sets approaches offer distinct advantages and challenges in aneurysm detection and segmentation. Surface mesh methods excel in precise morphological analysis but rely on accurate vascular model reconstruction and may struggle with identifying multiple aneurysms. DL-based point set methods provide accurate segmentation but require manual preprocessing and may miss details, particularly in smaller aneurysms. Both approaches underscore the complexity and potential of 3D geometric data, emphasizing the need for ongoing innovation and evaluation to maximize benefits in aneurysm analysis.

### 6. Approaches based on volumetric data

This section provides a summary of the studies using volumetric data as input for aneurysm detection and segmentation. As indicated in Table 5, most image-based methods aim to detect or localize aneurysms without quantification or morphological analysis. As detection is the

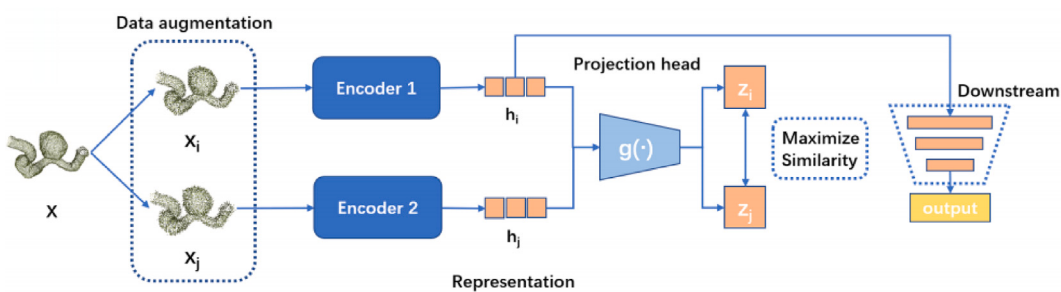


**Fig. 9.** The self-supervised learning framework for aneurysm detection using point sets. A point set is augmented to obtain a pair  $(x_i, x_j)$ , fed to the dual-branch encoders for contrastive learning by maximizing the similarity of the representation vectors  $z_i, z_j$ . The learned representation of vessels  $h$  is used for downstream tasks such as aneurysm classification.

Source: Image from Shao et al. (2022).

first step of aneurysm management, accurate detection at the beginning can assist clinicians in better diagnosis and decision-making. Volumetric data have advantages over 2D images because an additional dimension of the subject anatomy allows one to more accurately visualize the morphology of an aneurysm and possibly avoid misinterpretation. We divide this section into two parts: The first part describes methods requiring manual feature extraction and the second subsection is dedicated to DL-based methods.

#### 6.1. Non DL-based methods

We refer to all methods requiring manually extracted features without using deep neural networks as non DL-based methods. Researchers conduct distance analysis, extract shape features, or use deformable models without explicit feature extraction to distinguish aneurysms from other structures in volumetric data.

##### 6.1.1. Distance analysis

Since the introduction of Guglielmi detachable coils (GDC) for aneurysm treatment by Guglielmi et al. (1991), optimizing projection angles in DSA for accurate aneurysm parameter estimation has been crucial, especially to minimize contrast agent use and accurately view aneurysm necks for effective coiling procedures. Early efforts by van der Weide et al. (1998) and Wilson et al. (1999) focused on using distance maps and ray casting to detect the aneurysm neck plane, facilitating the selection of optimal imaging angles for treatment planning. Bruijns iteratively refined the distance-based analysis approach to quantify aneurysms in 3DRA images, employing distance transforms and ray casting to refine aneurysm isolation and neck detection (Bruijns, 2003, 2005). Later, the author and his research team incorporated shape information to correct the aneurysm boundary extracted from tubular approximations of the parent vessels (Bruijns et al., 2007). Karmonik et al. (2004) explored vessel diameter variations to isolate aneurysms. (Hassan et al., 2011) adopted a similar approach, using graph-based methods for precise neck identification.

The task of aneurysm isolation is often tackled as ostium or neck detection in surface-based approaches but rarely in image-based or voxel-based approaches. Cárdenes et al. (2011) proposed an automatic voxel-based framework for aneurysm neck detection, in which the neck is defined as a closed geodesic curve. They demonstrated the robustness of the framework across various aneurysm sizes and configurations by utilizing the fast marching method, but the method may generate an incorrect neck curve for multi-lobular aneurysms.

Hanaoka et al. (2015) introduces the HoTPiG (histogram of triangular paths in the graph) feature set to encode vessel voxels with shape information, leveraging these features in conjunction with an SVM and connected component analysis to determine the lesion likelihood.

##### 6.1.2. Shape analysis

Aneurysm detection often relies on shape analysis to differentiate between spherical aneurysms and tubular vessels. While the shape of a structure is directly linked to the morphology on surface models, in image data the shape is encoded by the intensity variations. Despite the difference, the morphology of vasculature can still be analyzed in volumetric data. Kang et al. (2008) applied an energy-based tube model to obtain a smoothed centerline and normal vessel, such that aneurysms or stenosis can be quantified. Kobashi et al. (2006) construct a healthy artery model using a thinning line and the estimated radii to identify ROI containing aneurysms and estimate a fuzzy degree for each aneurysm candidate based on case-based reasoning using shape and intensity features.

Lauric et al. (2010) introduced a shape descriptor called *writhe number* to distinguish between tubular and non-tubular regions along the vessels for aneurysm detection independent of image modality. The writhe number is defined by normal vectors for the neighborhood of each point on the vasculature. To account for different image resolutions, the region index (the product between the size of the region in voxels and the volume of the voxel) is used to reduce FPs, as true aneurysms tend to have a larger region index. The approach identified both saccular and fusiform aneurysms with a 100% detection rate. However, challenges remain in accurately identifying irregularly shaped aneurysms, as noted by Kohout et al. (2013).

Another shape-based strategy is using *enhancement filters* to amplify the intensity profile of circular structures, allowing aneurysm detection in multi-modal images. Enhancement filters are usually based on the eigenvalues of Hessian matrices, which describe the second-order local image intensity variations around a selected pixel or voxel. Eigenvalue decomposition can be used to evaluate the structure of a local region. For more information about the process, please refer to Frangi et al. (1998).

Several researchers (Arimura et al., 2004, 2006; Hentschke et al., 2011; Yang et al., 2011; Suniga et al., 2012; Hentschke et al., 2012, 2014; Nomura et al., 2014; Jerman et al., 2015b; Hu et al., 2020) utilized Hessian-based enhancement filters to identify aneurysm candidates and applied rule-based scheme or feature classification to remove FPs. A framework utilizing enhancement filtering (Jerman et al., 2015b) is illustrated in Fig. 10. The issues with typical enhancement filters are that the response of the filtered image is usually not uniform and that multi-scaling is required to identify spherical structures of various sizes.

Jerman et al. (2015a) introduced a novel enhancement filter that achieves uniform response within blob-like structures, enhancing TPs and suppressing FPs through a volume rendering method sensitive to signal energy. Building on this, Hu et al. (2020) proposed a multi-scale blob enhancement filter with parameters fine-tuned through Bayesian optimization, enabling the iterative detection of multiple aneurysms in 3D DSA images.

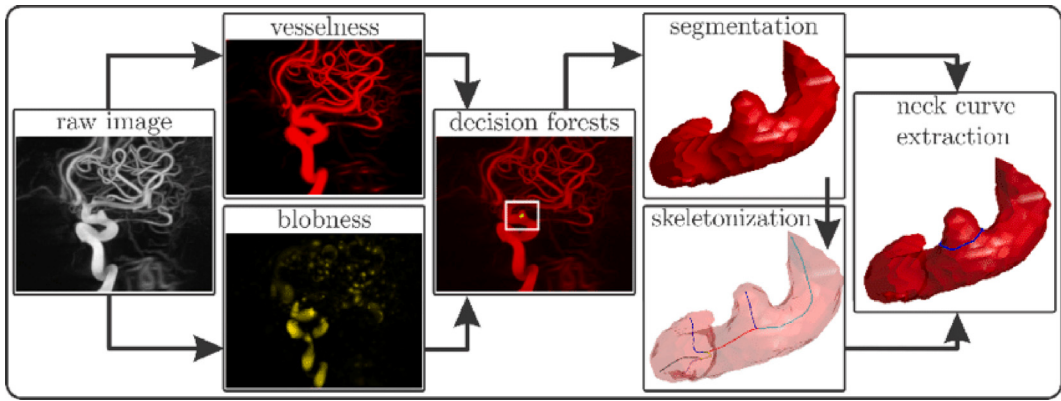


**Fig. 10.** An aneurysm detection, segmentation, and neck extraction framework based on a 3D DSA. The responses from the Hessian-based blobness and vesselness enhancement filters are used to locate the region of interest containing an aneurysm.  
Source: Image from Jerman et al. (2015b).

In addition to Hessian-based filters, gradient concentrate (GC) filters based on iris filter (Kobatake and Murakami, 1996) can also enhance rounded convex regions by measuring the degree of convergence of the gradient vectors around a point of interest. The iris filter evaluates the degree of convergence of the gradient vectors to detect convex regions, which works even with low contrast between the object of interest and the background. Uchiyama et al. (2006) proposed a CAD scheme for aneurysm detection in MRA using a GC filter to identify regions of interest in segmented vessels. The size, sphericity, and mean value of the GC image of the candidate regions were used by quadratic discriminant analysis to remove FPs.

With the advances in imaging technology, angiography has a higher image quality. In particular, MRA taken with a stronger magnetic field (3T) can visualize subtle vascular structures, leading to higher FPs in aneurysm detection using blob enhancement filtering (Jin et al., 2016). To avoid excessive FPs, Jin et al. (2016) developed an ellipsoid convex enhancement (ECE) filter to selectively enhance local intensity convex regions based on quadratic approximation using the eigenvalues of the Hessian matrix. The limitation is that the ECE filter was designed to detect aneurysms smaller than 7 mm in diameter.

#### 6.1.3. Deformable models

Deformable models are a collection of techniques for image segmentation based on contours (2D curves or 3D surfaces) which can be deformed according to some user-defined energy function to match particular regions. One common way to drive contour deformation is by the minimization of an objective function defined by internal and external energy:

$$E(\mathbf{X}(s)) = \int_0^1 E_{int}(\mathbf{X}(s)) + E_{ext}(\mathbf{X}(s)) ds \quad (9)$$

where  $\mathbf{X} = [x(s), y(s), z(s)]^T$  is the coordinates of the contour parameterized by  $s$ . The energies are governed by image intensity, gradient magnitude, and intensity variance. The internal energy keeps the contour smooth while the external energy tries to move the contour to the object boundary in the image. For aneurysm segmentation in volumetric images, an initial surface can be defined as a sphere inside the aneurysm sac. The deformable model approach requires vessel segmentation, and diffusion filters are often used for smoothing and preserving edges to enhance performance (Firouzian et al., 2011).

Nikravanshalmani et al. (2010) demonstrated the efficacy of level sets, an implicit deformable model, for aneurysm segmentation in CTA images. The authors later combined 3D conditional morphology segmentation based on predefined intensity range and anatomical information, and edge-based level set to iteratively refine the aneurysm segmentation from vessel-segmented CTA images (Nikravanshalmani et al., 2013). However, they only showed the result visually without

quantitative metrics. Chen et al. (2014) proposed a Lattice Boltzmann geodesic active contour method (LBGM) for giant aneurysm segmentation in CTA images in order to estimate both the volumes of the thrombus and the aneurysm. Anisotropic diffusion filtering smooths while preserving edges, and Canny edge detection enhances them, both applied in pre-processing to strengthen weak edges.

#### 6.2. DL-based methods

DL-based methods for aneurysm detection have been increasingly popular since 2017 (Jerman et al., 2017). With the automatic feature learning of deep neural networks, different image modalities can be processed using the same network architecture but with varying pre-processing steps. In particular, CNNs excel in image analysis due to their ability to recognize grid patterns and extract relevant features automatically using convolution operations. Depending on the architecture, CNNs can be used for classification (with fully connected layers at the end) or segmentation (fully convolutional networks, FCNs). FCNs were designed to take input of arbitrary size and generate a correspondingly-sized mask for semantic segmentation (Long et al., 2015). The networks usually have an encoding path to extract features from an input image and a decoding path to upsample the feature maps and restore the image resolution to output a segmentation mask. The skip connections between the two paths integrate different levels of features for inference. One of the most popular network architectures is U-Net, developed for biomedical imaging segmentation (Ronneberger et al., 2015), as shown in Fig. 11.

**3DRA.** Jerman et al. (2017) proposed the first DL-based system for image-based aneurysm detection. With small datasets of 15 3D DSA images, the authors apply a Hessian-based filter and 2D intra-vascular distance maps (IVDMs) to train a 2D CNN, achieving a 100% sensitivity with 2.4 FPs per dataset.

The Cerebral Aneurysm Detection and Analysis (CADA) challenge brought about several studies, most of which are based on 3D U-Net architecture, enabling both detection and segmentation. A comparison of different methods is shown in Table 7. Methods varied from employing reduced-sized U-Nets with vessel segmentation masks (Ivantits et al., 2020b), to leveraging attention mechanisms and pre-training strategies such as models genesis (Zhou et al., 2019d) to enhance spatial structure learning (Jia et al., 2020; Su et al., 2020). Jia et al. (2020) refined the result using the random forest classification for radiomic features (Van Griethuysen et al., 2017). Radiomics quantifies textural information in medical imaging through mathematical analysis of the distribution and correlations of signal intensities. Contrary to other studies using small image patch sizes, Ma and Nie (2020) used a relatively large image patch size as input of 3D nnU-Net (Isensee et al.,

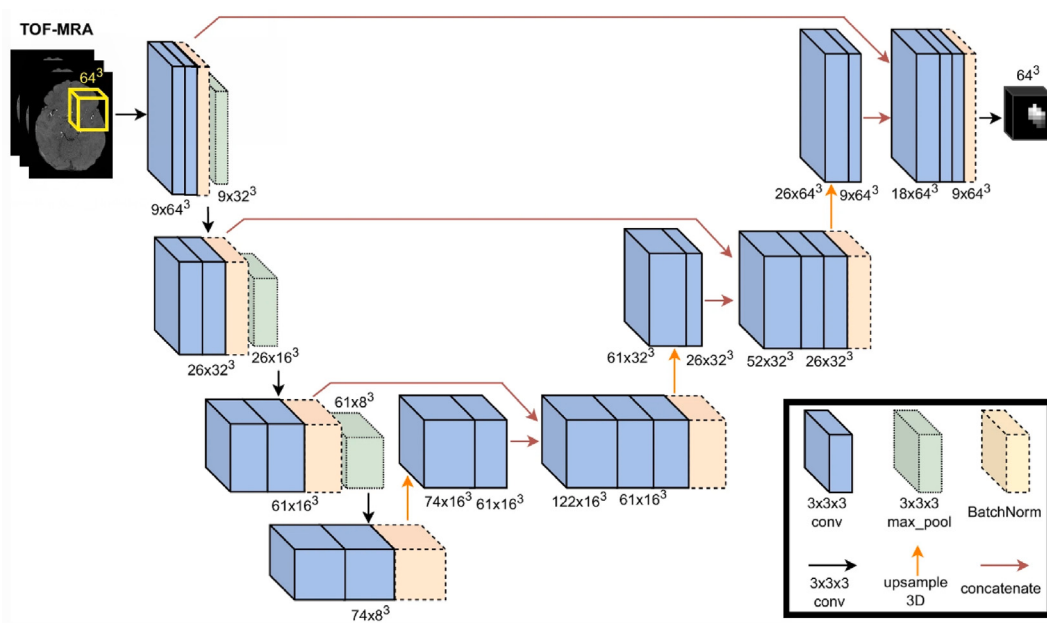


**Fig. 11.** A typical architecture of 3D U-Net, in which an encoding path and a decoding path form a U shape. It is common to use image patches as input for aneurysm detection and segmentation.

Source: Image from Di Noto et al. (2022).

**Table 7**  
Comparison of the performance of deep learning models on the CADA challenge datasets.

Ref.	Task	DL model	Input size	Sensitivity (FPs/case), Dice
Ivantsits et al. (2020b)	Detection	U-Net	28 × 28 × 28	0.869 (0.39), 0.84
Jia et al. (2020)	Detection	Attention U-Net	56 × 56 × 56	0.971 <sup>a</sup>
Su et al. (2020)	Segmentation	Attention U-Net	64 × 64 × 64	–, 0.907
Ma and Nie (2020)	Segmentation	nnU-Net	192 × 224 × 192	–, 0.886
Shi et al. (2020)	Segmentation	U-Net	128 × 128 × 128	–, 0.823
Li et al. (2022)	Segmentation	U-Net	96 × 96	–, 0.944
Lin et al. (2023)	Segmentation	U-Net++	64 × 64 × 64	–, 0.874

<sup>a</sup> Mean average precision (mAP).

2021) for aneurysm segmentation, aiming to extract more semantic context information.

Some approaches focused on the challenges of class imbalance and the differentiation of neighboring aneurysms through innovative strategies like gradient entropy for patch selection (Li et al., 2022) and custom modules within 3D U-Net++ (Zhou et al., 2019c) frameworks for improved feature extraction and segmentation accuracy (Lin et al., 2023). The custom modules include a transformer block (sensitive to subtle vascular structures), multi-view blocks (sensitive to continuous and slender features), and a learnable downsample block that retains subtle features during downsampling operations in a CNN-like architecture.

**CTA.** HeadXNet (Park et al., 2019) emerged as the pioneering DL-based aneurysm detection system based on CTA images, employing an encoder-decoder architecture akin to U-Net with strategies (auxiliary loss, weighted sampling, and freeze parameters for pure background input) to address class imbalance. The authors reported a boost of 0.059 in the clinicians' mean patient-level sensitivity. Ma et al. (2021) targeted the challenge of detecting small aneurysms by introducing a pipeline that enriches features through 3D to 2D projection. The authors utilized both a faster R-CNN (Ren et al., 2015) (detection) and a V-Net (Milletari et al., 2016) (segmentation), achieving a sensitivity of 0.8 for aneurysms ≤ 4 mm but moderate segmentation accuracy.

Shahzad et al. (2020) adapted the DeepMedic network from Kamnitsas et al. (2017), initially for brain lesion segmentation, to aneurysm detection, leveraging dual-path processing for integrating diverse feature

scales, resulting in notable sensitivity and accuracy.

In one of the largest cohort studies, Shi et al. (2020) deployed DAResUNet, highlighting the impact of image quality and scanner type on detection performance, with varying sensitivities and Dice scores across cohorts. The performance of the approach showed a wide range of sensitivity (0.606–0.956) and Dice scores (0.45–0.75) in five internal cohorts and three external medical centers. Another multi-center study was carried out by Bo et al. (2021), who introduced the global localization-based IA Network (GLIA-Net), focusing on segmenting aneurysms without manual pre- or post-processing, showing superior performance over U-Net and HeadXNet, though challenges remain in identifying small aneurysms (especially ≤ 3 mm). Yang et al. (2021) utilized a ResNet-18 enhanced with convolution block attention modules (CBAMs) (Woo et al., 2018) to detect both saccular and fusiform aneurysms. A patient-level sensitivity of 97.5% was reported, and eight new aneurysms overlooked in initial reports were identified by the algorithm. Wang et al. (2023) explored the effectiveness of single-phase versus multi-phase CTA for aneurysm detection using a 3D DAResUNet, assessing the capability to detect saccular, fusiform as well as ruptured and unruptured aneurysms. They reported better performance with multi-phase CTA, achieving a sensitivity of 0.97 with 0.649 FPs per case. A systematic review of DL-based aneurysm detection in CTA can be found in Bizjak and Špiclin (2023).

**MRA.** MRA is the most widely used volumetric imaging modality for aneurysm detection, particularly the non-invasive TOF-MRA. Nakao et al. (2018) proposed one of the first DL-based methods for aneurysm

**Table 8**

Comparison of the performance of deep learning models on the ADAM challenge datasets.

Ref	Task	DL model	Input Size	Sensitivity (FPs/case), DSC
Baumgartner et al. (2020)	Detection	Retina U-Net	224 × 224 × 56	0.66 (0.14)
Di Noto et al. (2022)	Detection	3D U-Net	64 × 64 × 64	0.680 (2.5)
Ye et al. (2022)	Segmentation	OTO-Net	128 × 128 × 64	–, 0.9813
Yuan et al. (2022)	Segmentation	DCAU-Net	64 × 64 × 64	0.788, 0.746
Zhou and Huang (2022)	Segmentation	IntrAsegTran	128 × 144 × 80	0.911 (0.1), 0.580

detection in MRA images. The authors adopted a 2D CNN to process concatenated MIP images extracted from volumes of interest (VOIs).

The rise of 3D U-Net variants has further propelled detection and segmentation capabilities (Baumgartner et al., 2020; Chen et al., 2020; Assis et al., 2021). Noteworthy advancements include the use of a 3D Retina U-Net (Jaeger et al., 2020) by Baumgartner et al. (2020), who excelled in the ADAM challenge (Timmins et al., 2021) by a patient-level sensitivity of 0.67 with 0.14 FPs. The framework integrates features across scales for segmentation and aggregates the features from the segmentation branch for aneurysm detection. Di Noto et al. (2022) developed a weakly supervised detection framework using an anatomically informed selection of MRA patches as input (Fig. 11), in which the weak labels are spheres containing the aneurysm annotated by radiologists. The authors provided their source code and the annotated data as open source. Yuan et al. (2022) utilized dense blocks and CBAMs to construct a dense convolutional attention U-Net (DCAU-Net) for aneurysm segmentation. DCAU-Net reached a Dice score of 0.746 on the ADAM challenge datasets, outperforming many models (DeepMedic, HeadXNet, GLIA-Net, DAREsUnet, U-Net) on segmentation of aneurysm with a diameter smaller than 7 mm. Ye et al. (2022) proposed the one-two-one fully convolutional network (ONO-Net) using three continuous encoding and decoding structures, achieving a Dice score of 0.981 for aneurysm segmentation on the ADAM challenge datasets. Table 8 compares the performance of methods validating ADAM datasets. More details of the works from the participants of the ADAM challenge can be found in Timmins et al. (2021).

Other popular network architectures include DeepMedic (Sichtermann et al., 2019; Faron et al., 2020) and ResNet (Ueda et al., 2019; Joo et al., 2020; Shimada et al., 2020). The studies (Sichtermann et al., 2019; Ueda et al., 2019) evaluated their approach with external datasets and reported a detection sensitivity of over 90%. The limitations include low specificity and low sensitivity to heterogeneous, as well as small or large aneurysms that are rare in the training datasets; however, the papers did not provide any concrete values for these limitations. Besides, the subjects recruited for the datasets did not include any healthy controls. Joo et al. (2020) adopted a similar strategy as in Ueda et al. (2019) by patch-based training using ResNet for aneurysm detection. They achieved a relatively low sensitivity of 85.7% but a high specificity of 98.0% in the external test set. The differences may be due to the vessel segmentation in the pre-processing steps and the inclusion of healthy controls in the training data. Joo et al. (2020) also introduced a pixel voting algorithm at the end of the network to reduce FPs.

Hou et al. (2020) introduced a computationally efficient 1D CNN for aneurysm detection, achieving a 95.9% accuracy. By transforming 2D MIP images into 576-element vectors through a pixel accumulation projection algorithm, this method reduces data size to 14.1% of the original 3D data.

Most CNN models have issues with small object detection because of the deep convolutional layers through which the impacts of small distant objects decay. Zhou and Huang (2022) introduced intrAsegTran, a transformer-based framework, to improve small aneurysm detection, achieving a sensitivity of 91.1% with 0.1 FPs per case, but the overall DSC is only 0.58 on the ADAM dataset.

### 6.3. Summary of volumetric data approaches

This section reviews methods for aneurysm detection and segmentation using volumetric data. Non-DL approaches employ distance analysis, shape analysis, or deformable models, often requiring additional steps like vessel segmentation or enhancement. DL-based methods, particularly leveraging 3D U-Net architectures since 2017, have shown promise due to advancements in automatic feature learning. Challenges persist in accurately identifying small aneurysms and ensuring model generalization. Notably, DL-based methods, despite not universally offering faster or more accurate performance, often undergo validation across extensive datasets, including multi-center datasets. Continued advancements in DL techniques hold promise for enhancing clinical applications.

## 7. Approaches based on 2D images

Although 2D images have a limited view of the vasculature, numerous studies demonstrated their effectiveness in detecting, segmenting, or analyzing aneurysms morphologically. DSA has long been considered the gold standard for aneurysm detection because of its high spatial and temporal resolution with superior sensitivity. Thus, most papers used 2D DSA images as input. Given that DSA images are commonly acquired in sequences during contrast agent injection, some studies leverage this temporal aspect for enhanced aneurysm analysis (Zakaria et al., 2011; Jin et al., 2019; Liao et al., 2019; Zeng et al., 2019). The algorithms of aneurysm analysis of 2D images can be categorized into non-DL-based and DL-based.

### 7.1. Non-DL-based methods

Non-DL-based algorithms usually start with vessel segmentation to extract morphological or intensity-based features essential for aneurysm analysis. The most common strategy for vessel segmentation is thresholding, which can be a simple global threshold or more advanced Frangi filtering to enhance the major vessels and anomalies. Following initial vessel extraction, morphological operations like erosion and dilation contribute to the rapid and accurate detection (Mitra and Chandra, 2013; Chandra and Mondal, 2017) and segmentation (Mondal and Chandra, 2014) of aneurysms, although validation is typically limited to small datasets (fewer than 20) with clearly visible aneurysms. Rahmany and Khelifa (2014) applied fuzzy logic for aneurysm detection, enhancing vasculature visualization using fuzzy classifiers followed by fuzzy opening to identify blob-like aneurysms. Mitra and Chandra (2013) developed a detection pipeline using a modified Hough circle transform (MHCT) to identify aneurysms by analyzing peaks in a 3D parameter space, like peak trekking in a mountain range. The limitations of their approach include a small number of datasets (12) and the requirement of manual parameter tuning.

It is also common to use a rule-based method based on the assumptions of aneurysm characteristics. Sulayman et al. (2016) proposed a three-step algorithm to segment aneurysms in DSA. The first two steps include a series of filtering (Gaussian, Frangi, and custom filters) for vessel enhancement and combining Otsu's thresholding and morphological processing for ROI identification. Sulayman et al. (2016) used

a combination of filters and morphological processing for aneurysm segmentation. Afterwards, a rule-based classifier based on shape features (circularity, solidity, and eccentricity) was used to remove FPs. However, the applicability across different aneurysm sizes remains uncertain. Rahmany et al. (2018a) utilized a combination of feature descriptors, i.e. maximally stable extremal regions (MSER), speed-up robust features (SURF), and scale-invariant feature transform (SIFT), along with fuzzy logic to detect aneurysms of various sizes. The mechanism lies in the analysis of DSA images through overlapping windows of varying dimensions for the feature descriptors. The extracted shape features were fused to reduce FPs.

One of the earliest studies of automated methods using DSA images identified aneurysms based on the calculation of time to peak (TTP) and time duration (TD) of the flow of contrast agent in blood vessels from DSA sequence (Zakaria et al., 2011). TTP is the time required for the contrast agent in the blood to fill a segment of the blood vessel, which can be used to segment vessels. TD is the period during which the contrast agent is maintained inside the blood vessel. A longer TD indicates a higher probability of an aneurysm. The authors showed that medium aneurysms can be identified using the two temporal parameters.

Frameworks capable of identifying both saccular and fusiform aneurysms focused on extracting textural features (Rahmany et al., 2019; Zafar et al., 2021). Rahmany et al. (2019) use local binary patterns (LBPs) with k-nearest neighbor (KNN) classifier for the determination of initial aneurysm candidates, and generic Fourier descriptor (GFD), a region-based shape descriptor based on contours, for false positive removal. Zafar et al. (2021) trained a KNN classifier on a feature vector combining shape and texture features, including circularity, eccentricity, and Haralick features derived from a Gray-Level Co-occurrence Matrix (GLCM), achieving a detection accuracy of 95% and a location classification accuracy of 82.6%. Both studies showed the feasibility of supervised learning with a bunch of shape and texture features in detecting aneurysms of different shapes and sizes. However, the performance depends on the image quality or precise vasculature extraction. Besides, the approach is computationally expensive, as it requires the extraction of image patches and the computation of textural features.

## 7.2. DL-based methods

Most DL-based algorithms for aneurysm detection require only basic pre-processing steps without vessel enhancement or segmentation. The most basic deep neural network architecture is the multilayer perceptron (MLP), which consists of at least three layers (input, hidden, output) of artificial neurons interconnected between two adjacent layers. Because of the simple architecture, MLP still requires manually extracted features for image analysis. Malik et al. (2018) proposed a detection and quantification framework for aneurysms in DSA images. They employed watershed segmentation and distance transformation for ROI extraction and trained an MLP with Haralick features to classify ROIs. They introduced the BASSH score for assessing aneurysm rupture risk. Extending this work to include more data and multimodal images (DSA and MRA) yielded a 98% classification accuracy, and a 76.67% rupture prediction accuracy, though it was not tested on images with multiple or small aneurysms (<5 mm).

Researchers demonstrated the efficacy of automated aneurysm segmentation using FCN variants (Podgorsak et al., 2020; Kashyap et al., 2022; Stember et al., 2019). Instead of using DSA images, Stember et al. (2019) took the maximum intensity projection (MIP) of MRA as input images trained a 20-layer U-Net to segment aneurysms and measured the size of basilar tip aneurysms, the aneurysms with the highest rupture risk (Al-Sharydah et al., 2021). On average, the estimated aneurysm size differed from radiologist-annotated aneurysm size by 2.01 mm (30%).

To make use of the temporal information in the DSA sequence, researchers combined *long short-term memory* (LSTM) (Hochreiter and Schmidhuber, 1997) with CNN to detect aneurysms (Duan et al., 2019; Liao et al., 2019; Jin et al., 2019). Liao et al. (2019) developed a two-stage framework incorporating cascaded feature pyramid networks (FPNs) to initially pinpoint ROIs from DSA sequences, followed by utilizing FPNs alongside bi-directional LSTM for spatio-temporal feature extraction. This approach achieved an 88% sensitivity with a time cost of 3.664s per case, but was limited to aneurysms in the *posterior communicating artery* (PCom) region. Jin et al. (2019) enhanced U-Net with bi-directional convolutional LSTM modules to capture the change in contrast medium flow, reaching 89.3% sensitivity in less than a second per DSA sequence.

DSA sequences can also be obtained from the rotational angiography sequence (sinograms), where each projection image corresponds to a slightly different view of the vasculature (Fig. 12), highlighting morphological differences as a major feature (Zeng et al., 2019). Using such a sequence avoids errors induced by thresholding and 3D reconstruction. Moreover, 2D DSA is superior to 3DRA for measuring morphological descriptors such as dome-to-neck ratio (Brinjikji et al., 2009). Zeng et al. (2019) proposed an aneurysm detection framework based on a spatial information fusion (SIF) method, where consecutive projection image ROIs are vertically merged into a single image. The authors used a modified VGG16 to train the concatenated images and got a detection accuracy of 98.89%. However, the approach's effectiveness diminishes with the use of more than six frames due to significant viewpoint shifts, and it struggles to accurately identify aneurysms smaller than 3 mm or those situated closely together.

## 7.3. Summary of 2D image-based approaches

This section explores methods for detecting aneurysms using 2D images. While these images offer a limited view of blood vessels, they have proven effective for aneurysm identification. Non-DL methods typically involve vessel segmentation, using techniques like thresholding and morphological operations. DL-based approaches skip segmentation and directly analyze images using architectures like FPNs and U-Nets. The temporal information from DSA sequences can enhance 2D methods for improved detection accuracy. Challenges include accurately detecting small aneurysms and generalizing models across datasets. Overall, while 2D approaches show potential, they are not as prevalent or promising as their 3D counterparts.

## 8. Discussion

Computer-aided diagnosis of intracranial aneurysms has evolved for more than two decades. As shown in Fig. 13, volumetric data is primarily used for aneurysm detection, especially in 2020 when the CADA and ADAM challenges encouraged researchers to conduct experiments using publicly accessible datasets. Surface meshes have been less frequently used. From the previous sections, we can observe the trend of the algorithms of aneurysm detection: automaticity, end-to-end, and multiplicity. Automaticity refers to the automatic process without user interaction. This is especially the case for surface-based algorithms where automatic methods replace manual vessel segmentation and ROIs. End-to-end is a term used in the machine learning community to describe a method that solves a learning task in a single step. For aneurysm detection, DL-based methods are usually end-to-end without the steps that many non-DL-based methods require, such as vessel segmentation and FP removal. Multiplicity indicates that algorithms can identify multiple aneurysms without iteration over different ROIs. With the progress of deep learning, most recent CAD systems are enhanced by the automatic feature learning capability of DL-based algorithms that shape the trend in aneurysm detection and segmentation. All the discussed algorithms belong to CAD systems, meaning that they are designed to assist rather than replace clinicians. Some studies showed the

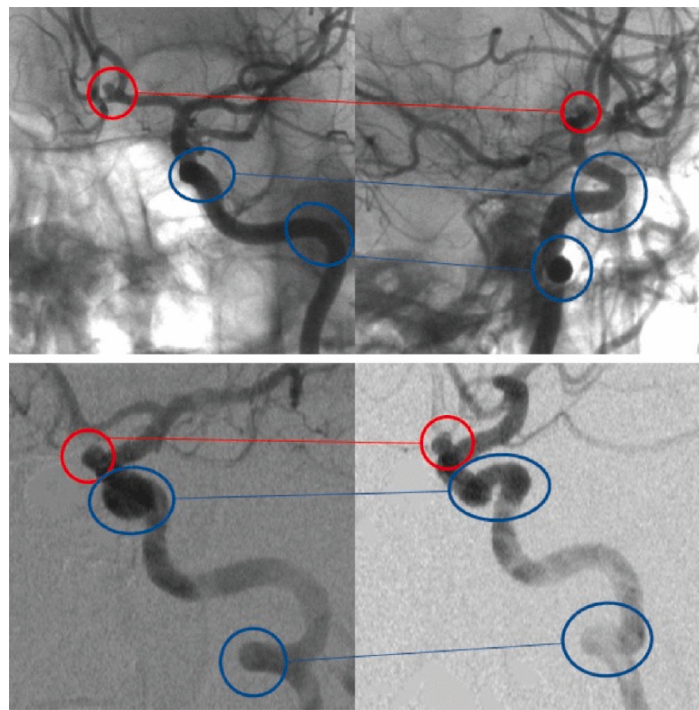


**Fig. 12.** Aneurysms and overlapping vessels require different viewpoints to be distinguished in 2D images. Aneurysms are marked in red circles and vascular overlaps are marked in blue circles.

Source: Image from Zeng et al. (2019).

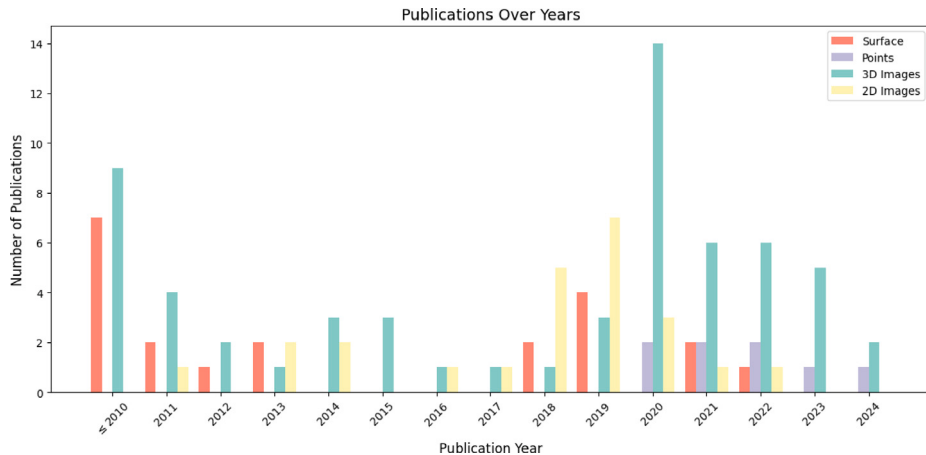


**Fig. 13.** The publications on aneurysm detection and segmentation in the past two decades are categorized by the input data format.

efficacy of CAD systems in augmenting the radiologists' performance or identifying tricky cases in which aneurysms were overlooked by human experts (Štepán-Buksakowska et al., 2014; Park et al., 2019; Yang et al., 2021). It is noteworthy that CAD systems can assist the radiologists in image interpretation, but do not necessarily reduce the reading time for diagnosis (Din et al., 2023).

We can roughly divide the aneurysm detection and segmentation frameworks into either surface-based or image-based approaches. Surface-based approaches are suitable for quantitative analysis as the shape information can be derived directly from surface models. They usually rely on the extracted skeleton of vascular structures to identify the abnormal shapes that indicate a high possibility of aneurysms. The vessel and centerline extraction procedures exhibit both advantages and disadvantages. They allow the vascular data to be modality-agnostic and easier for morphological analysis. On the other hand, they require extra computation power and manual work and may

introduce processing errors. Point-based approaches can be considered as a subset of surface-based approaches, as the point data are directly obtained from the vertices of surface models. As point sets lose the connectivity information, they are restricted to detection or segmentation and not suitable for morphological analysis. Most image-based approaches aim at aneurysm detection and segmentation, using distance or shape analysis to identify abnormal vascular structures. Distance and shape are inherently gray-level features in images, so they are dependent on image modalities, scanners, and pre-processing methods. These approaches can detect multiple aneurysms by first identifying many aneurysm candidates and removing false aneurysms through a rule-based scheme or discriminant analysis, which still quite often leaves some FPs untouched. Powerful deep learning algorithms, especially CNN-based neural networks, have been widely used for aneurysm analysis. Unlike classical methods that rely on manual feature extraction, DL-based methods focus on automatic feature learning,

streamlining the CAD workflow but often facing challenges in decision interpretation. That is, how a deep neural network detects aneurysms is a black box process, so the association between the extracted features and the pathology and aneurysm morphology is unclear.

Even with the advanced techniques integrated into the CAD systems, aneurysm detection remains a challenging task. In particular, current studies indicate a relatively low sensitivity in detecting small and irregular aneurysms. Moreover, a considerable number of FPs occur. The most fundamental reasons lie in the varying sizes of aneurysms as well as the complex vascular structure and diverse aneurysm morphology. These challenges are associated with imaging techniques, detection methods, and the collected data. Since the imaging techniques are beyond the scope of this survey, we will take a look at some limitations from the perspectives of the methods and data.

Most aneurysm detection systems were retrospectively validated without clear data description, meaning that the datasets are prone to selection bias. The only studies that collected data prospectively are (Duan et al., 2019; Hu et al., 2024). Moreover, most studies relied on a 'limited number of datasets'—a term frequently used but not clearly defined in deep learning literature—to design and validate their approaches. This practice may lead to reported high accuracy in cases involving many regular and large aneurysms, or it may result in low sensitivity when the datasets include special or atypical cases. Another common caveat, especially in early studies, is the collection of datasets only from patients with a single aneurysm. Those studies should be considered as proofs of concept but may not be applicable in clinical settings. Some studies attempted to include datasets from different imaging devices or from multiple institutions (Ueda et al., 2019; Shi et al., 2020; Bo et al., 2021; Yang et al., 2021), which requires cooperation between research and medical institutions and should be the trend for future studies. More details of the quality assessment of some of the studies can be found in the previous review papers (Gu et al., 2022; Din et al., 2023; Bizjak and Špiclin, 2023).

Regarding the methodology, there are some limitations that are noteworthy. One comes from the study assumptions that restrict the search space for an aneurysm detection system. One of the most common assumptions is the spherical shape of aneurysms. While saccular aneurysms are much more prevalent than fusiform ones and usually circular, there are inevitably some special cases in which aneurysms have irregular shapes, wide necks, or multiple lobules. Besides, complex vessel structures may fool algorithms with shape assumptions to detect many FPs at branching sites of small cerebral arteries or tightly curving carotid siphons (Hanaoka et al., 2015). In surface-based approaches, the ostium is often assumed to be the narrowest place between the aneurysm and parent vessel, which can be found by optimization but can lead to inaccurate quantitative analysis. Apart from assumptions, many studies were designed to directly process vasculature segments to avoid the issue of data imbalance and the need for ROI extraction. As mentioned in Yang et al. (2023), using fragments as input data is unrealistic in clinical practice. A practical way would be to take the whole intracranial vessel network or angiography as input and use patch-based methods to sample the input for aneurysm localization and analysis. The inherent issue with DL-based methods is a lack of model and decision interpretation. Several techniques using saliency maps, feature attribution, and perturbation-based methods have been proposed for deep learning models in image analysis. The interpretability of DL-based aneurysm analysis has yet to be explored to better understand how deep neural networks identify aneurysms. In addition, many DL-based studies are limited to the same network architectures, such as U-Net and ResNet for image-based and MeshCNN for surface-based approaches. Recent studies have tried implementing successful frameworks like transformer (Yu et al., 2021; Li et al., 2022; Zhou and Huang, 2022) or a novel method (Hou et al., 2020) to process image data. For surface meshes, there are definitely more options than MeshCNN (Wang and Zhang, 2022), e.g. graph-based methods in the spatial or spectral domain (Zhou et al., 2020). A survey of graph neural

networks (GNNs) for computer vision tasks can be found in Chen et al. (2022). Moreover, text-vision frameworks show promise for detecting brain abnormalities from unlabeled MRI scans (Wood et al., 2024), laying groundwork for multi-task systems to diagnose aneurysms alongside conditions like thrombosis. Integrating large language models (LLMs) can further improve accuracy, leveraging prior knowledge to overcome limited clinical datasets (Zhou et al., 2024).

This survey summarized the available studies of aneurysm detection and segmentation methods. The proposed taxonomy provides an overview of the evolution of methods and the trend of this research topic. We did not quantitatively compare different approaches, as the studies we included used slightly different evaluation metrics with various purposes. Even with the same metric for evaluation, like detection sensitivity, we could not compare these approaches on the same level because the sensitivity was based on different criteria, e.g., lesion-level versus patient-level sensitivity and FPs per case. Besides, they were validated on different datasets. Therefore, we only listed the metrics in Tables 4–6 and had Tables 7 and 8 to compare a few studies using the same open datasets. We encourage interested readers to read the reviews in Gu et al. (2022), Din et al. (2023) and Bizjak and Špiclin (2023) for statistical evaluation of studies focusing on automated aneurysm detection. Hopefully, readers can have a grasp of the available methods for automatic aneurysm detection and segmentation. They can design their own framework according to their resources such as imaging devices and datasets. As a final remark, one should ensure that the designed CAD system should aid the clinicians instead of replacing them or increasing their work with excessive false detection.

## 9. Conclusions

This paper provides a comprehensive survey of semi-automated and automated detection and segmentation of intracranial aneurysms. Our taxonomy categorized these approaches based on data, tasks, and methodology, revealing trends towards increased automation, end-to-end processing, and handling of multiple aneurysms. Despite significant progress, current systems still struggle with detecting small and irregularly shaped aneurysms, highlighting the need for more diverse datasets collected from various scanners and institutions to mitigate selection bias. The methods should also refrain from too many assumptions or fragment-based training to be implemented in clinical practice.

Looking ahead, the advancements in imaging modalities, such as improvements in 3D angiography (3DRA, multidetector CTA, and MRA), are promising. These developments, coupled with the advancement of deep learning techniques, particularly CNN-based architectures for imaging data and geometric DL for surface or point-based data, are poised to benefit from enhanced image resolution and more accurate quantification methods. However, careful consideration of potential drawbacks, such as increased computational complexity and the need for robust validation and interpretation of DL-based models, is essential to ensure the successful integration of these advancements into clinical practice.

## CRediT authorship contribution statement

**Wei-Chan Hsu:** Writing – review & editing, Writing – original draft, Visualization, Investigation, Formal analysis, Conceptualization. **Monique Meuschke:** Writing – review & editing, Writing – original draft, Conceptualization. **Alejandro F. Frangi:** Writing – review & editing. **Bernhard Preim:** Writing – review & editing. **Kai Lawonn:** Writing – review & editing, Writing – original draft, Supervision, Conceptualization.

## Declaration of competing interest

The authors declare that they have no known competing financial interests or personal relationships that could have appeared to influence the work reported in this paper.

## Data availability

No data was used for the research described in the article.

## References

- Al-Sharydah, A., Al-Abdulwahhab, A., Al-Suhibani, S., Al-Muhanna, A., Abohimed, A., Al-Sharidah, A., Alabbas, F., 2021. The analysis of morphoradiological parameters in predicting risk of basilar artery tip aneurysm rupture: a retrospective cohort study. *Int. J. Gen. Med.* 14, 3335.
- Anjum, S.M., Malik, K.M., Soltanian-Zadeh, H., Malik, H., Malik, G., 2018. Saccular brain aneurysm detection and multiclassifier rupture prediction using digital subtraction and magnetic resonance angiograms. In: Proc. of International Conference on Biomedical and Bioinformatics Engineering. pp. 87–94.
- Apilla, V., Behrendt, B., Lawonn, K., Preim, B., Meuschke, M., 2021. Automatic animations to analyze blood flow data. In: Proc. of Visual Computing for Biology and Medicine. pp. 101–105.
- Arimura, H., Li, Q., Korogi, Y., Hirai, T., Abe, H., Yamashita, Y., Katsuragawa, S., Ikeda, R., Doi, K., 2004. Automated computerized scheme for detection of unruptured intracranial aneurysms in three-dimensional magnetic resonance angiography1. *Academic Radiol.* 11, 1093–1104.
- Arimura, H., Li, Q., Korogi, Y., Hirai, T., Katsuragawa, S., Yamashita, Y., Tsuchiya, K., Doi, K., 2006. Computerized detection of intracranial aneurysms for three-dimensional mr angiography: Feature extraction of small protrusions based on a shape-based difference image technique. *Med. Phys.* 33, 394–401.
- Asikainen, A., Korja, M., Kaprio, J., Rautalin, I., 2023. Case fatality in patients with aneurysmal subarachnoid hemorrhage in finland: a nationwide register-based study. *Neurology* 100, e348–e356.
- Assis, Y., Liao, L., Pierre, F., Anzionnat, R., Kerrien, E., 2021. An efficient data strategy for the detection of brain aneurysms from mra with deep learning. In: Deep Generative Models, and Data Augmentation, Labelling, and Imperfections. Springer, pp. 226–234.
- Assis, Y., Liao, L., Pierre, F., Anzionnat, R., Kerrien, E., 2023. Aneurysm pose estimation with deep learning. In: Proc. of Medical Image Computing and Computer-Assisted Intervention. Springer, pp. 543–553.
- Baumgartner, M., Jaeger, P., Isensee, F., Maier-Hein, K.H., 2020. Retina u-net for aneurysm detection in mr images. *Autom. Detect. Segm. Chall. ( ADAM)*.
- Beaman, C., Patel, S.D., Nael, K., Colby, G.P., Liebeskind, D.S., 2023. Imaging of intracranial saccular aneurysms. *Stroke: Vasc. Interv. Neurol.* 3, e000757.
- Bizjak, Ž., Choi, J.H., Park, W., Špiclin, Ž., 2022. Deep learning based modality-independent intracranial aneurysm detection. In: Proc. of Medical Image Computing and Computer-Assisted Intervention. Springer, pp. 760–769.
- Bizjak, Ž., Likar, B., Pernuš, F., Špiclin, Ž., 2020. Vascular surface segmentation for intracranial aneurysm isolation and quantification. In: Proc. of Medical Image Computing and Computer Assisted Intervention. Springer, pp. 128–137.
- Bizjak, Ž., Likar, B., Pernuš, F., Špiclin, Ž., 2021. Modality agnostic intracranial aneurysm detection through supervised vascular surface classification. In: Proc. of Medical Imaging 2021: Computer-Aided Diagnosis. SPIE, pp. 161–168.
- Bizjak, Ž., Špiclin, Ž., 2023. A systematic review of deep-learning methods for intracranial aneurysm detection in CT angiography. *Biomedicines* 11, 2921.
- Bo, Z.H., Qiao, H., Tian, C., Guo, Y., Li, W., Liang, T., Li, D., Liao, D., Zeng, X., Mei, L., et al., 2021. Toward human intervention-free clinical diagnosis of intracranial aneurysm via deep neural network. *Patterns* 2, 100197.
- Bogunović, H., Pozo, J.M., Villa-Uriol, M.C., Majoe, C.B., van den Berg, R., Gratama van Andel, H.A., Macho, J.M., Blasco, J., San Román, L., Frangi, A.F., 2011. Automated segmentation of cerebral vasculature with aneurysms in 3dra and tof-mra using geodesic active regions: an evaluation study. *Med. Phys.* 38, 210–222.
- Brinjikji, W., Cloft, H., Lanzino, G., Kallmes, D., 2009. Comparison of 2D digital subtraction angiography and 3D rotational angiography in the evaluation of dome-to-neck ratio. *Am. J. Neuroradiol.* 30, 831–834.
- Bruyns, J., 2003. Fully-automatic labelling of aneurysm voxels for volume estimation. In: Proc. of Bildverarbeitung FÜR Die Medizin. Springer, pp. 51–55.
- Bruyns, J., 2005. Local distance thresholds for enhanced aneurysm labelling. In: Proc. of Bildverarbeitung FÜR Die Medizin. Springer, pp. 148–152.
- Bruyns, J., Peters, F.J., Berretty, R., Barenbrug, B., 2007. Fully-automatic correction of the erroneous border areas of an aneurysm. In: Proc. of Bildverarbeitung FÜR Die Medizin. Springer, pp. 293–297.
- Cao, W., Chen, X., Lv, J., Shao, L., Si, W., 2024b. Semi-supervised intracranial aneurysm segmentation via reliable weight selection. *Vis. Comput.* 1–13.
- Cao, R., Zhang, D., Wei, P., Ding, Y., Zheng, C., Tan, D., Zhou, C., 2024a. Pmmnet: A dual branch fusion network of point cloud and multi-view for intracranial aneurysm classification and segmentation. *IEEE J. Biomed. Heal. Inform.*
- Cárdenes, R., Larrabide, I., Román, L.S., Frangi, A.F., 2013. Performance assessment of isolation methods for geometrical cerebral aneurysm analysis. *Med. Biol. Eng. Comput.* 51, 343–352.
- Cárdenes, R., Pozo, J.M., Bogunovic, H., Larrabide, I., Frangi, A.F., 2011. Automatic aneurysm neck detection using surface voronoi diagrams. *IEEE Trans. Med. Imaging* 30, 1863–1876.
- Cebral, J.R., Mut, F., Weir, J., Putman, C.M., 2011. Association of hemodynamic characteristics and cerebral aneurysm rupture. *Am. J. Neuroradiol.* 32, 264–270.
- Chandra, A., Mondal, S., 2017. Amalgamation of iterative double automated thresholding and morphological filtering: a new proposition in the early detection of cerebral aneurysm. *Multimedia Tools Appl.* 76, 23957–23979.
- Chappell, E.T., Moure, F.C., Good, M.C., 2003. Comparison of computed tomographic angiography with digital subtraction angiography in the diagnosis of cerebral aneurysms: a meta-analysis. *Neurosurgery* 52, 624–631.
- Chen, Y., Navarro, L., Wang, Y., Courbebaisse, G., 2014. Segmentation of the thrombus of giant intracranial aneurysms from ct angiography scans with lattice boltzmann method. *Med. Image Anal.* 18, 1–8.
- Chen, G., Wei, X., Lei, H., Liqin, Y., Yuxin, L., Yakang, D., Daoying, G., 2020. Automated computer-assisted detection system for cerebral aneurysms in time-of-flight magnetic resonance angiography using fully convolutional network. *BioMed. Eng. OnLine* 19, 1–10.
- Chen, C., Wu, Y., Dai, Q., Zhou, H.Y., Xu, M., Yang, S., Han, X., Yu, Y., 2022. A survey on graph neural networks and graph transformers in computer vision: A task-oriented perspective. *arXiv preprint arXiv:2209.13232*.
- Chowriappa, A., Salunke, S., Mokin, M., Kan, P., Scott, P.D., 2013. 3D vascular decomposition and classification for computer-aided detection. *IEEE Trans. Biomed. Eng.* 60, 3514–3523.
- Claux, F., Baudouin, M., Bogey, C., Rouchaud, A., 2023. Dense, deep learning-based intracranial aneurysm detection on tof mri using two-stage regularized U-Net. *J. Neuroradiol.* 50, 9–15.
- Dai, X., Huang, L., Qian, Y., Xia, S., Chong, W., Liu, J., Di Ieva, A., Hou, X., Ou, C., 2020. Deep learning for automated cerebral aneurysm detection on computed tomography images. *Int. J. Comput. Assist. Radiol. Surg.* 15, 715–723.
- Dhar, S., Tremmel, M., Mocco, J., Kim, M., Yamamoto, J., Siddiqui, A.H., Hopkins, L.N., Meng, H., 2008. Morphology parameters for intracranial aneurysm rupture risk assessment. *Neurosurgery* 63, 185–197.
- Di Noto, T., Marie, G., Tourbier, S., Alemán-Gómez, Y., Esteban, O., Saliou, G., Cuadra, M.B., Hagmann, P., Richiardi, J., 2022. Towards automated brain aneurysm detection in tof-mra: open data, weak labels, and anatomical knowledge. *Neuroinformatics* 1–14.
- Dim, M., Agarwal, S., Grzeda, M., Wood, D.A., Modat, M., Booth, T.C., 2023. Detection of cerebral aneurysms using artificial intelligence: a systematic review and meta-analysis. *J. NeuroInterventional Surg.* 15, 262–271.
- do Carmo, M., 1976. Differential Geometry of Curves and Surfaces. Prentice-Hall, Differential Geometry of Curves and Surfaces.
- Duan, H., Huang, Y., Liu, L., Dai, H., Chen, L., Zhou, L., 2019. Automatic detection on intracranial aneurysm from digital subtraction angiography with cascade convolutional neural networks. *Biomed. Eng. Online* 18, 1–18.
- El Hamdaoui, H., Maaroufi, M., Alami, B., Chaoui, N., Boujraf, S., 2017. Computer-aided diagnosis systems for detecting intracranial aneurysms using 3d angiographic data sets. In: Proc. of International Conference on Advanced Technologies for Signal and Image Processing: ATSiP, IEEE, pp. 1–5.
- Etiminan, N., Rinkel, G.J., 2016. Unruptured intracranial aneurysms: development, rupture and preventive management. *Nat. Rev. Neurol.* 12, 699–713.
- Eulzer, P., Meuschke, M., Mistelbauer, G., Lawonn, K., 2022. Vessel Maps: A survey of map-like visualizations of the cardiovascular system. *Comput. Graph. Forum* 41, 645–673.
- Faluk, M., De Jesus, O., 2022. Saccular aneurysm. In: StatPearls [Internet]. StatPearls Publishing.
- Faron, A., Sichtermann, T., Teichert, N., Luetkens, J.A., Keulers, A., Nikoubashman, O., Freiherr, J., Mpotsaris, A., Wiesmann, M., 2020. Performance of a deep-learning neural network to detect intracranial aneurysms from 3d tof-mra compared to human readers. *Clin. Neuroradiol.* 30, 591–598.
- Felde, J., Wagner, T., Lamecker, H., Doenitz, C., Gundelwein, L., 2021. Automatic vessel segmentation and aneurysm detection pipeline for numerical fluid analysis. In: Proc. of Bildverarbeitung FÜR Die Medizin. Springer, pp. 247–252.
- Firouzian, A., Manniesing, R., Flach, Z.H., Risselada, R., van Kooten, F., Sturkenboom, M.C., van der Lugt, A., Niessen, W.J., 2011. Intracranial aneurysm segmentation in 3D CT angiography: Method and quantitative validation with and without prior noise filtering. *Eur. J. Radiol.* 79, 299–304.
- Ford, M., Hoi, Y., Piccinelli, M., Antiga, L., Steinman, D., 2009. An objective approach to digital removal of saccular aneurysms: technique and applications. *Br. J. Radiol.* 82, S55–S61.
- Frangi, A.F., Niessen, W.J., Vincken, K.L., Viergever, M.A., 1998. Multiscale vessel enhancement filtering. In: Proc. of Medical Image Computing and Computer-Assisted Intervention. Springer, pp. 130–137.
- Gasparotti, R., Liserre, R., 2005. Intracranial aneurysms. *Eur. Radiol.* 15, 441–447.
- Glaßer, S., Lawonn, K., Hoffmann, T., Skalej, M., Preim, B., 2014. Combined visualization of wall thickness and wall shear stress for the evaluation of aneurysms. *IEEE Trans. Vis. Comput. Graphics* 250, 6–2515.
- Goni, M.R., Ruhaiyem, N.I.R., Mustapha, M., Achuthan, A., Nassir, C.M.N.C.M., 2022. Brain vessel segmentation using deep learning—a review. *IEEE Access* 10, 111322–111336.
- Greving, J.P., Werner, M.J., Brown, Jr., R.D., Morita, A., Juvela, S., Yonetkura, M., Ishibashi, T., Torner, J.C., Nakayama, T., Rinkel, G.J., et al., 2014. Development of the PHASES score for prediction of risk of rupture of intracranial aneurysms: a pooled analysis of six prospective cohort studies. *Lancet Neurol.* 13, 59–66.

- Gu, F., Wu, X., Wu, W., Wang, Z., Yang, X., Chen, Z., Wang, Z., Chen, G., 2022. Performance of deep learning in the detection of intracranial aneurysm: a systematic review and meta-analysis. *Eur. J. Radiol.* 155, 110457.
- Guglielmi, G., Vilueta, F., Sepetka, I., Macellari, V., 1991. Electrotrombosis of saccular aneurysms via endovascular approach: part 1: electrochemical basis, technique, and experimental results. *J. Neurosurg.* 75, 1–7.
- Guo, M.H., Cai, J.X., Liu, Z.N., Mu, T.J., Martin, R.R., Hu, S.M., 2021. Pct: Point cloud transformer. *Comput. Vis. Media* 7, 187–199.
- Hainc, N., Mannil, M., Anagnostakou, V., Alkadihi, H., Blüthgen, C., Wacht, L., Bink, A., Husain, S., Kulcsár, Z., Winklhofer, S., 2020. Deep learning based detection of intracranial aneurysms on digital subtraction angiography: a feasibility study. *Neuroradiol. J.* 33, 311–317.
- Ham, S., Seo, J., Yun, J., Bae, Y.J., Kim, T., Sunwoo, L., Yoo, S., Jung, S.C., Kim, J.W., Kim, N., 2023. Automated detection of intracranial aneurysms using skeleton-based 3d patches, semantic segmentation, and auxiliary classification for overcoming data imbalance in brain tof-mra. *Sci. Rep.* 13, 12018.
- Hanaoka, S., Nomura, Y., Nemoto, M., Miki, S., Yoshikawa, T., Hayashi, N., Ohtomo, K., Masutani, Y., Shimizu, A., 2015. HoTPiG: a novel geometrical feature for vessel morphometry and its application to cerebral aneurysm detection. In: Proc. of Medical Image Computing and Computer-Assisted Intervention. Springer, pp. 103–110.
- Hanocka, R., Hertz, A., Fish, N., Giryes, R., Fleishman, S., Cohen-Or, D., 2019. Meshcnn: a network with an edge. *ACM Trans. Graph.* 38, 1–12.
- Hassan, S., Hétry, F., Faure, F., Palombi, O., 2011. Automatic localization and quantification of intracranial aneurysms. In: Proc. of International Conference on Computer Analysis of Images and Patterns. Springer, pp. 554–562.
- Hentschke, C.M., Beuing, O., Nickl, R., Tönnies, K.D., 2011. Automatic cerebral aneurysm detection in multimodal angiographic images. In: Proc. of IEEE Nuclear Science Symposium Conference Record. pp. 3116–3120.
- Hentschke, C.M., Beuing, O., Paukisch, H., Scherlach, C., Skalej, M., Tönnies, K.D., 2014. A system to detect cerebral aneurysms in multimodality angiographic data sets. *Med. Phys.* 41, 091904.
- Hentschke, C.M., Tönnies, K.D., Beuing, O., Nickl, R., 2012. A new feature for automatic aneurysm detection. In: Proc. of IEEE International Symposium on Biomedical Imaging. ISBI, pp. 800–803.
- Hernandez, M., Frangi, A.F., 2007. Non-parametric geodesic active regions: method and evaluation for cerebral aneurysms segmentation in 3dra and cta. *Med. Image Anal.* 11, 224–241.
- Hochreiter, S., Schmidhuber, J., 1997. Long short-term memory. *Neural Comput.* 9, 1735–1780.
- Hou, Z., 2006. A review on MR image intensity inhomogeneity correction. *Int. J. Biomed. Imaging* 2006.
- Hou, W., Mei, S., Gui, Q., Zou, Y., Wang, Y., Deng, X., Cheng, Q., 2020. 1D cnn-based intracranial aneurysms detection in 3d tof-mra. *Complexity* 2020.
- Howard, B.M., Hu, R., Barrow, J.W., Barrow, D.L., 2019. Comprehensive review of imaging of intracranial aneurysms and angiographically negative subarachnoid hemorrhage. *Neurosurg. Focus*. 47, E20.
- Hu, B., Shi, Z., Lu, L., Miao, Z., Wang, H., Zhou, Z., Zhang, F., Wang, R., Luo, X., Xu, F., et al., 2024. A deep-learning model for intracranial aneurysm detection on ct angiography images in china: a stepwise, multi-centre, early-stage clinical validation study. *Lancet Digit. Heal.* 6, e261–e271.
- Hu, T., Yang, H., Ni, W., Lei, Y., Jiang, Z., Shi, K., Yu, J., Gu, Y., Wang, Y., 2020. Automatic detection of intracranial aneurysms in 3d-dsa based on a bayesian optimized filter. *BioMed. Eng. OnLine* 19, 1–18.
- Iavindrasana, J., Iacono, L.L., Müller, H., Periz, I., Summers, P., Wright, J., Friedrich, C.M., Dach, H., Gattermayer, T., Engelbrecht, G., et al., 2008. The@ neurIST project. *Stud. Health Technol. Inform.* 138, 161–164.
- Isensee, F., Jaeger, P.F., Kohl, S.A., Petersen, J., Maier-Hein, K.H., 2021. nnU-Net: a self-configuring method for deep learning-based biomedical image segmentation. *Nature Methods* 18, 203–211.
- Ishibashi, T., Murayama, Y., Urashima, M., Saguchi, T., Ebara, M., Arakawa, H., Irie, K., Takao, H., Abe, T., 2009. Unruptured intracranial aneurysms: incidence of rupture and risk factors. *Stroke* 40, 313–316.
- Ivantits, M., Goubergrits, L., Kuhnigk, J.M., Huellebrand, M., Brüning, J., Kossen, T., Pfahringer, B., Schaller, J., Spuler, A., Kuehne, T., et al., 2020a. Cerebral aneurysm detection and analysis challenge 2020 (cada). In: Proc. of International Workshop on Cerebral Aneurysm Detection. Springer, pp. 3–17.
- Ivantits, M., Kuhnigk, J.M., Huellebrand, M., Kuehne, T., Hennemuth, A., 2020b. Deep learning-based 3d u-net cerebral aneurysm detection. In: Proc. of International Workshop on Cerebral Aneurysm Detection. Springer, pp. 31–38.
- Jaeger, P.F., Kohl, S.A., Bickelhaupt, S., Isensee, F., Kuder, T.A., Schlemmer, H.P., Maier-Hein, K.H., 2020. Retina U-Net: Embarrassingly simple exploitation of segmentation supervision for medical object detection. In: Proc. of Machine Learning for Health Workshop. PMLR, p. 17.
- Jang, M., Kim, J.H., Park, J.W., Roh, H., Lee, H.J., Seo, J., Hwang, S.H., Yoon, J.H., Yoon, S.H., Cho, B.K., 2020. Features of false positive unruptured intracranial aneurysms on screening magnetic resonance angiography. *PLoS One* 15, e0238597.
- Jerman, T., Chien, A., Pernuš, B., Špiclin, Ž., 2019. Automated cutting plane positioning for intracranial aneurysm quantification. *IEEE Trans. Biomed. Eng.* 67, 577–587.
- Jerman, T., Pernuš, F., Likar, B., Špiclin, Ž., 2017. Aneurysm detection in 3d cerebral angiograms based on intra-vascular distance mapping and convolutional neural networks. In: Proc. of IEEE International Symposium on Biomedical Imaging (ISBI 2017). pp. 612–615.
- Jerman, T., Pernuš, B., Špiclin, Ž., 2015a. Blob enhancement and visualization for improved intracranial aneurysm detection. *IEEE Trans. Vis. Comput. Graphics* 22, 1705–1717.
- Jerman, T., Pernuš, B., Špiclin, Ž., 2015b. Computer-aided detection and quantification of intracranial aneurysms. In: Proc. of International Conference on Medical Image Computing and Computer-Assisted Intervention. Springer, pp. 3–10.
- Jerman, T., Pernuš, B., Špiclin, Ž., Chien, A., 2016. Automatic cutting plane identification for computer-aided analysis of intracranial aneurysms. In: Proc. of International Conference on Pattern Recognition. ICPR, IEEE, pp. 1484–1489.
- Jia, Y., Liao, W., Lv, Y., Su, Z., Dou, J., Sun, Z., Li, X., 2020. Detect and identify aneurysms based on adjusted 3D attention UNet. In: Proc. of International Workshop on Cerebral Aneurysm Detection. Springer, pp. 39–48.
- Jin, Z., Arimura, H., Kakeda, S., Yamashita, F., Sasaki, M., Korogi, Y., 2016. An ellipsoid convex enhancement filter for detection of asymptomatic intracranial aneurysm candidates in CAD frameworks. *Med. Phys.* 43, 951–960.
- Jin, H., Yin, Y., Hu, M., Yang, G., Qin, L., 2019. Fully automated unruptured intracranial aneurysm detection and segmentation from digital subtraction angiography series using an end-to-end spatiotemporal deep neural network. In: Proc. of Medical Imaging 2019: Image Processing. SPIE, pp. 379–386.
- Joo, B., Ahn, S.S., Yoon, P.H., Bae, S., Sohn, B., Lee, Y.E., Bae, J.H., Park, M.S., Choi, H.S., Lee, S.K., 2020. A deep learning algorithm may automate intracranial aneurysm detection on mr angiography with high diagnostic performance. *Eur. Radiol.* 30, 5785–5793.
- Kamnitsas, K., Ledig, C., Newcombe, V.F., Simpson, J.P., Kane, A.D., Menon, D.K., Rueckert, D., Glocker, B., 2017. Efficient multi-scale 3D CNN with fully connected crf for accurate brain lesion segmentation. *Med. Image Anal.* 36, 61–78.
- Kang, D.G., Suh, D.C., Ra, J.B., 2008. Three-dimensional blood vessel quantification via centerline deformation. *IEEE Trans. Med. Imaging* 28, 405–414.
- Karmonik, C., Arat, A., Benndorf, G., Akpek, S., Klucznik, R., Mawad, M.E., Strother, C.M., 2004. A technique for improved quantitative characterization of intracranial aneurysms. *Am. J. Neuroradiol.* 25, 1158–1161.
- Kashyap, S., Bulu, H., Jadhav, A., Dholakia, R., Liu, A.Y., Rangwala, H., Patterson, W.R., Moradi, M., 2022. A new deep neural segmentation network for cerebral aneurysms in 2D digital subtraction angiography. In: Proc. of Medical Imaging 2022: Image-Guided Procedures, Robotic Interventions, and Modeling. SPIE, pp. 8–14.
- Keedy, A., 2006. An overview of intracranial aneurysms. *McGill J. Med.: MJM* 9, 141.
- Kirbas, C., Quek, F., 2004. A review of vessel extraction techniques and algorithms. *ACM Comput. Surv.* 36, 81–121.
- Kobashi, S., Kondo, K., Hata, Y., 2006. Computer-aided diagnosis of intracranial aneurysms in mra images with case-based reasoning. *IEICE Trans. Inf. Syst.* 89, 340–350.
- Kobatake, H., Murakami, M., 1996. Adaptive filter to detect rounded convex regions: Iris filter. In: Proc. of International Conference on Pattern Recognition. IEEE, pp. 340–344.
- Koenderink, J.J., Van Doorn, A.J., 1992. Surface shape and curvature scales. *Image Vis. Comput.* 10, 557–564.
- Kohout, J., Chiarini, A., Clapworthy, G.J., Klajnšek, G., 2013. Aneurysm identification by analysis of the blood-vessel skeleton. *Comput. Methods Programs Biomed.* 109, 32–47.
- Ku, J.C., Pasarikovski, C.R., Dobashi, Y., Ramjist, J., Priola, S.M., Yang, V.X., 2022. Review of intraluminal optical coherence tomography imaging for cerebral aneurysms. *Front. Photon.* 3, 1015661.
- Labuz-Roszak, B., Skrzypek, M., Starostka-Tatar, A., Lasek-Bal, A., Gąsior, M., Gierlotka, M., 2022. Subarachnoid Haemorrhage—Incidence of hospitalization, management and case fatality rate—in the Silesian Province, Poland, in the Years 2009–2019. *J. Clin. Med.* 11, 4242.
- Larrabide, I., Villa-Urio, M.C., Cardenes, R., Pozo, J.M., Hose, D.R., Frangi, A.F., 2010. Automated intracranial aneurysm isolation and quantification. In: Proc. of IEEE Engineering in Medicine and Biology. pp. 2841–2844.
- Larrabide, I., Villa-Urio, M.C., Cárdenes, R., Pozo, J.M., Macho, J., Roman, L.S., Blasco, J., Vivas, E., Marzo, A., Hose, D.R., et al., 2011. Three-dimensional morphological analysis of intracranial aneurysms: A fully automated method for aneurysm sac isolation and quantification. *Med. Phys.* 38, 2439–2449.
- Lauric, A., Miller, E., Friskin, S., Malek, A.M., 2010. Automated detection of intracranial aneurysms based on parent vessel 3D analysis. *Med. Image Anal.* 14, 149–159.
- Law, M.W., Chung, A.C., 2012. Segmentation of intracranial vessels and aneurysms in phase contrast magnetic resonance angiography using multirange filters and local variances. *IEEE Trans. Image Process.* 22, 845–859.
- Lawonn, K., Gasteiger, R., Preim, B., 2013. Adaptive surface visualization of vessels with embedded blood flow based on the suggestive contour measure. In: Proc. of VMV. pp. 113–120.
- Lawonn, K., Gasteiger, R., Preim, B., 2014. Adaptive surface visualization of vessels with animated blood flow. *Comput. Graph. Forum* 33 (8), 16–27.
- Lawonn, K., Glaßer, A., Preim, B., Isenberg, T., 2015. Occlusion-free blood flow animation with wall thickness visualization. *IEEE Trans. Vis. Comput. Graphics* 22 (1), 728–737.

- Lawonn, K., Meuschke, M., Wickenhöfer, R., Preim, B., Hildebrandt, K., 2019. A geometric optimization approach for the detection and segmentation of multiple aneurysms. *Comput. Graph. Forum* 38, 413–425. <http://dx.doi.org/10.1111/cgf.13699>.
- Li, T., An, X., Di, Y., He, J., Liu, S., Ming, D., 2022. Segmentation method of cerebral aneurysms based on entropy selection strategy. *Entropy* 24, 1062.
- Li, J., Chen, B.M., Lee, G.H., 2018. So-net: Self-organizing network for point cloud analysis. In: Proc. of the IEEE Conference on Computer Vision and Pattern Recognition. pp. 9397–9406.
- Liao, J., Duan, H., Dai, H., Huang, Y., Liu, L., Chen, L., Zhou, L., 2019. Automatic detection of intracranial aneurysm from digital subtraction angiography with cascade networks. In: Proc. of International Conference on Artificial Intelligence and Pattern Recognition. pp. 18–23.
- Lin, F., Xia, Y., Song, S., Ravikumar, N., Frangi, A.F., 2023. High-throughput 3Dra segmentation of brain vasculature and aneurysms using deep learning. *Comput. Methods Programs Biomed.* 107355.
- Liu, X., Feng, J., Wu, Z., Neo, Z., Zhu, C., Zhang, P., Wang, Y., Jiang, Y., Mitsouras, D., Li, Y., 2021. Deep neural network-based detection and segmentation of intracranial aneurysms on 3d rotational DSA. *Interv. Neuroradiol.* 27, 648–657.
- Liu, Y., Zheng, Y., An, Q., Song, Y., Leng, B., 2019. Optical coherence tomography for intracranial aneurysms: a new method for assessing the aneurysm structure. *World Neurosurg.* 123, e194–e201.
- Long, J., Shelhamer, E., Darrell, T., 2015. Fully convolutional networks for semantic segmentation. In: Proc. of IEEE Conference on Computer Vision and Pattern Recognition. pp. 3431–3440.
- Ma, B., Harbaugh, R.E., Raghavan, M.L., 2004. Three-dimensional geometrical characterization of cerebral aneurysms. *Ann. Biomed. Eng.* 32, 264–273.
- Ma, J., Nie, Z., 2020. Exploring large context for cerebral aneurysm segmentation. In: Proc. of International Workshop on Cerebral Aneurysm Detection. Springer, pp. 68–72.
- Ma, R., Tu, S., Li, P., Zhou, J., Zhao, B., Wan, J., Xu, L., 2021. Enriching computed tomography images by projection for robust automated cerebral aneurysm detection and segmentation. In: Proc. of IEEE International Conference on Bioinformatics and Biomedicine. BIBM, pp. 1026–1031.
- Maier-Hein, L., Mountney, P., Bartoli, A., Elhawary, H., Elson, D., Groch, A., Kolb, A., Rodrigues, M., Sorger, J., Speidel, S., et al., 2013. Optical techniques for 3D surface reconstruction in computer-assisted laparoscopic surgery. *Med. Image Anal.* 17, 974–996.
- Maier-Hein, L., Reinke, A., Godau, P., Tizabi, M.D., Buettner, F., Christodoulou, E., Glocker, B., Isensee, F., Kleesiek, J., Kozubek, M., et al., 2024. Metrics reloaded: recommendations for image analysis validation. *Nature Methods* 1–18.
- Malik, K.M., Anjum, S.M., Soltanian-Zadeh, H., Malik, H., Malik, G.M., 2018. A framework for intracranial saccular aneurysm detection and quantification using morphological analysis of cerebral angiograms. *IEEE Access* 6, 7970–7986.
- Marasini, A., Shrestha, A., Phuyal, S., Zaidat, O.O., Kalia, J.S., 2022. Role of artificial intelligence in unruptured intracranial aneurysm: An overview. *Front. Neurol.* 22.
- Maupu, C., Lebas, H., Boulaftali, Y., 2022. Imaging modalities for intracranial aneurysm: More than meets the Eye. *Front. Cardiovasc. Med.* 9.
- McLaughlin, R.A., Noble, J.A., 2002. Demarcation of aneurysms using the seed and cull algorithm. In: Proc. of Medical Image Computing and Computer-Assisted Intervention. Springer, pp. 419–426.
- Meng, C., Yang, D., Chen, D., 2021. Cerebral aneurysm image segmentation based on multi-modal convolutional neural network. *Comput. Methods Programs Biomed.* 208, 106285.
- Mensah, E., Pringle, C., Roberts, G., Gurusingshe, N., Golash, A., Alalade, A.F., 2022. Deep learning in the management of intracranial aneurysms and cerebrovascular diseases: A review of the current literature. *World Neurosurg.*
- Meuschke, M., Engelke, W., Beuing, O., Preim, B., Lawonn, K., 2017a. Automatic viewpoint selection for exploration of time-dependent cerebral aneurysm data. In: Proc. of Bildverarbeitung FÜR Die Medizin. Springer, pp. 352–357.
- Meuschke, M., Günther, T., Berg, P., Wickenhöfer, R., Preim, B., Lawonn, K., 2019a. Visual analysis of aneurysm data using statistical graphics. *IEEE Trans. Vis. Comput. Graphics* 25, 997–1007.
- Meuschke, M., Günther, T., Berg, P., Wickenhöfer, R., Preim, B., Lawonn, K., 2018a. Visual analysis of aneurysm data using statistical graphics. *IEEE Trans. Vis. Comput. Graphics* 25, 997–1007.
- Meuschke, M., Günther, T., Wickenhöfer, R., Gross, M., Preim, B., Lawonn, K., 2018b. Management of cerebral aneurysm descriptors based on an automatic ostium extraction. *IEEE Comput. Graph. Appl.* 38, 58–72.
- Meuschke, M., Oeltze-Jafra, S., Beuing, O., Preim, B., Lawonn, K., 2019b. Classification of blood flow patterns in cerebral aneurysms. *IEEE Trans. Vis. Comput. Graphics* 25, 2404–2418.
- Meuschke, M., Preim, B., Lawonn, K., 2021a. Aneulysis – a system for the visual analysis of aneurysm data. *Comput. Graph..*
- Meuschke, M., Voß, S., Beuing, O., Preim, B., Lawonn, K., 2017b. Combined visualization of vessel deformation and hemodynamics in cerebral aneurysms. *IEEE Trans. Vis. Comput. Graphics* 23 (1), 761–770.
- Meuschke, M., Voß, S., Beuing, O., Preim, B., Lawonn, K., 2017c. Glyph-based comparative stress tensor visualization in Cerebral Aneurysms. *Comput. Graph. Forum* 36, 99–108.
- Meuschke, M., Voß, S., Eulzer, P., Janiga, G., Arens, C., Wickenhöfer, R., Preim, B., Lawonn, K., 2022. COMFIS-Comparative visualization of simulated medical flow data. In: Proc. of Visual Computing for Biology and Medicine. pp. 29–40.
- Meuschke, M., Voß, S., Gaidzik, F., Preim, B., Lawonn, K., 2021b. Skyscraper visualization of multiple time-dependent scalar fields on surfaces. *Comput. Graph..*
- Meuschke, M., Voß, S., Preim, B., Lawonn, K., 2018c. Exploration of blood flow patterns in cerebral aneurysms during the cardiac cycle. *Comput. Graph.* 72, 12–25.
- Miki, S., Hayashi, N., Masutani, Y., Nomura, Y., Yoshikawa, T., Hanaoka, S., Nemoto, M., Ohtomo, K., 2016. Computer-assisted detection of cerebral aneurysms in MR angiography in a routine image-reading environment: effects on diagnosis by radiologists. *Am. J. Neuroradiol.* 37, 1038–1043.
- Milletari, F., Navab, N., Ahmadi, S.A., 2016. V-net: Fully convolutional neural networks for volumetric medical image segmentation. In: Proc. of International Conference on 3D Vision (3DV). IEEE, pp. 565–571.
- Mine, B., Pezzullo, M., Roque, G., David, P., Metens, T., Lubicz, B., 2015. Detection and characterization of unruptured intracranial aneurysms: Comparison of 3 t MRA and DSA. *J. Neuroradiol.* 42, 162–168.
- Mitra, J., Chandra, A., 2013. Detection of cerebral aneurysm by performing thresholding-spatial filtering-thresholding operations on digital subtraction angiogram. In: Advances in Computing and Information Technology. Springer, pp. 915–921.
- Mitra, J., Chandra, A., Halder, T., 2013. Peak trekking of hierarchy mountain for the detection of cerebral aneurysm using modified Hough circle transform. *ELCVIA: Electron. Lett. Comput. Vis. Image Anal.* 12, 57–84.
- Mohamed, A., Sgouritsa, E., Morsi, H., Shaltoni, H., Mawad, M.E., Kakadairis, I.A., 2010. Computer-aided planning for endovascular treatment of intracranial aneurysms (CAPETA). In: Proc. of Medical Imaging 2010: Visualization, Image-Guided Procedures, and Modeling. SPIE, pp. 968–976.
- Mondal, S., Chandra, A., 2014. One novel algorithm for the detection of cerebral aneurysm using morphological filtering. In: Proc. of International Conference on Communication and Signal Processing. IEEE, pp. 137–141.
- Nakao, T., Hanaoka, S., Nomura, Y., Sato, I., Nemoto, M., Miki, S., Maeda, E., Yoshikawa, T., Hayashi, N., Abe, O., 2018. Deep neural network-based computer-assisted detection of cerebral aneurysms in mr angiography. *J. Magn. Reson. Imaging* 47, 948–953.
- Neugebauer, M., Diehl, V., Skalej, M., Preim, B., 2010. Geometric reconstruction of the Ostium of Cerebral Aneurysms. In: Proc. of VMV. pp. 307–314.
- Neugebauer, M., Lawonn, K., Beuing, O., Berg, P., Janiga, G., Preim, B., 2013a. AmniVis - A system for qualitative exploration of near-wall hemodynamics in cerebral aneurysms. *Comput. Graph. Forum* 32 (3), 251–260.
- Neugebauer, M., Lawonn, K., Beuing, O., Preim, B., 2013b. Automatic generation of anatomic characteristics from cerebral aneurysm surface models. *Int. J. Comput. Assist. Radiol. Surg.* 8, 279–289.
- Ngoepe, M.N., Frangi, A.F., Byrne, J.V., Ventikos, Y., 2018. Thrombosis in cerebral aneurysms and the computational modeling thereof: a review. *Front. Physiol.* 9, 306.
- Niemann, A., Schneider, L., Preim, B., Voß, P., Saalfeld, S., 2021. Towards deep learning-based wall shear stress prediction for intracranial aneurysms. In: Proc. of Bildverarbeitung FÜR Die Medizin. Springer, pp. 105–110.
- Nikravanshalmani, A., Karamimohammadi, M., Dehmeshki, J., 2013. Segmentation and separation of cerebral aneurysms: A multi-phase approach. In: Proc. of International Symposium on Image and Signal Processing and Analysis. ISPA, IEEE, pp. 505–510.
- Nikravanshalmani, A., Qanadli, S.D., Ellis, T.J., Crocker, M., Ebrahimdoost, Y., Karamimohammadi, M., Dehmeshki, J., 2010. Three-dimensional semi-automatic segmentation of intracranial aneurysms in cta. In: Proc. of IEEE International Conference on Information Technology and Applications in Biomedicine. pp. 1–4.
- Nomura, Y., Masutani, Y., Miki, S., Nemoto, M., Hanaoka, S., Yoshikawa, T., Hayashi, N., Ohtomo, K., 2014. Performance improvement in computerized detection of cerebral aneurysms by retraining classifier using feedback data collected in routine reading environment. *J. Biomed. Graph. Comput.* 4, 12.
- Noto, T.D., Marie, G., Tourbier, S., Aleman-Gómez, Y., Esteban, O., Saliou, G., Cuadra, M.B., Haggmann, P., Richiardi, J., 2022. Lausanne TOF-MRA aneurysm cohort. <http://dx.doi.org/10.18112/openneuro.ds003949.v1.0.1>.
- Oeltze-Jafra, S., Meuschke, M., Neugebauer, M., Saalfeld, S., Lawonn, K., Janiga, G., Hege, H.C., Zachow, S., Preim, B., 2019. Generation and visual exploration of medical flow data: Survey, research trends and future challenges. *Comput. Graph. Forum* 1, 87–125.
- Otsu, N., 1979. A threshold selection method from gray-level histograms. *IEEE Trans. Syst. Man Cybern.* 9, 62–66.
- Padilla, R., Netto, S.L., Da Silva, E.A., 2020. A survey on performance metrics for object-detection algorithms. In: Proc. of International Conference on Systems, Signals and Image Processing. IWSSIP, IEEE, pp. 237–242.
- Park, A., Chute, C., Rajpurkar, P., Lou, J., Ball, R.L., Shpanskaya, K., Jabarkheel, R., Kim, L.H., McKenna, E., Tseng, J., et al., 2019. Deep learning-assisted diagnosis of cerebral aneurysms using the HeadXNet model. *JAMA Netw. Open* 2, e195600.
- Park, S.H., Yim, M.B., Lee, C.Y., Kim, E., Son, E.I., 2008. Intracranial fusiform aneurysms: its pathogenesis, clinical characteristics and managements. *J. Korean Neurosurg. Soc.* 44, 116.
- Piccinelli, M., Steinman, D.A., Hoi, Y., Tong, F., Veneziani, A., Antiga, L., 2012. Automatic neck plane detection and 3D geometric characterization of aneurysmal sacs. *Ann. Biomed. Eng.* 40, 2188–2211.

- Podgorsak, A.R., Rava, R.A., Bhurwani, M.M.S., Chandra, A.R., Davies, J.M., Sidiqui, A.H., Ionita, C.N., 2020. Automatic radiomic feature extraction using deep learning for angiographic parametric imaging of intracranial aneurysms. *J. Neurointerventional Surg.* 12, 417–421.
- Prasetya, H., Mengko, T., Santoso, O., Zakaria, H., 2011. Detection method of cerebral aneurysm based on curvature analysis from 3D medical images. In: Proc. of International Conference on Instrumentation, Communications, Information Technology, and Biomedical Engineering. IEEE, pp. 141–144.
- Prefßer, R., Lawonn, K., Preim, B., Meuschke, M., 2022. Virtual DSA visualization of simulated blood flow data in cerebral aneurysms. In: Proc. of Bildverarbeitung FÜR Die Medizin. Springer, pp. 241–246.
- Prefßer, R., Meuschke, M., Voigt, H., Lawonn, K., 2023. WEB-ANEULYSIS: A web-based application for the analysis of aneurysm data. In: Proc. of Bildverarbeitung für die Medizin. Springer, pp. 88–94.
- Qi, C.R., Su, H., Mo, K., Guibas, L.J., 2017a. Pointnet: Deep learning on point sets for 3d classification and segmentation. In: Proc. of the IEEE Conference on Computer Vision and Pattern Recognition. pp. 652–660.
- Qi, C.R., Yi, L., Su, H., Guibas, L.J., 2017b. Pointnet++: Deep hierarchical feature learning on point sets in a metric space. *Adv. Neural Inf. Process. Syst.* 30.
- Radaelli, A., Peiro, J., 2010. On the segmentation of vascular geometries from medical images. *Int. J. Numer. Methods Biomed. Eng.* 26, 3–34.
- Rahmany, I., Arfaoui, B., Khelifa, N., Megdiche, H., 2018a. Cerebral aneurysm computer-aided detection system by combining MSER, SURF and SIFT descriptors. In: Proc. of International Conference on Control, Decision and Information Technologies (CoDiIT). IEEE, pp. 1122–1127.
- Rahmany, I., Guetari, R., Khelifa, N., 2018b. A fully automatic based deep learning approach for aneurysm detection in DSA images. In: Proc. of IEEE International Conference on Image Processing, Applications and Systems. IPAS, pp. 303–307.
- Rahmany, I., Khelifa, N., 2014. Detection of intracranial aneurysm in angiographic images using fuzzy approaches. In: Proc. of International Image Processing, Applications and Systems Conference. IEEE, pp. 1–6.
- Rahmany, I., Khelifa, N., 2018. A priori knowledge integration for the detection of cerebral aneurysm. *Biomed. Engineering/Biomed. Tech.* 63, 445–452.
- Rahmany, I., Nemmala, M.E.A., Khelifa, N., Megdiche, H., 2019. Automatic detection of intracranial aneurysm using LBP and Fourier descriptor in angiographic images. *Int. J. Comput. Assist. Radiol. Surg.* 14, 1353–1364.
- Rauf, R.H.A., Ghafar, N.A., Khalid, N.E.A., 2019. Brain aneurysm extraction in MRI images. In: Proc. of Software and Computer Applications. pp. 286–290.
- Ren, S., He, K., Girshick, R., Sun, J., 2015. Faster r-cnn: Towards real-time object detection with region proposal networks. *Adv. Neural Inf. Process. Syst.* 28.
- Ronneberger, O., Fischer, P., Brox, T., 2015. U-net: Convolutional networks for biomedical image segmentation. In: Proc. of Medical Image Computing and Computer-Assisted Intervention. Springer, pp. 234–241.
- Saalfeld, S., Berg, P., Niemann, A., Luz, M., Preim, B., Beuing, O., 2018. Semiautomatic neck curve reconstruction for intracranial aneurysm rupture risk assessment based on morphological parameters. *Int. J. Comput. Assist. Radiol. Surg.* 13, 1781–1793.
- Sangalli, L.M., Secchi, P., Vantini, S., 2014. Aneurisk65: A dataset of three-dimensional cerebral vascular geometries. *Electron. J. Stat.* 8, 1879–1890.
- Schneider, L., Niemann, A., Beuing, O., Preim, B., Saalfeld, S., 2021. MedmeshCNN-enabling meshcnn for medical surface models. *Comput. Methods Programs Biomed.* 210, 106372.
- Sgouritsa, E., Mohamed, A., Morsi, H., Shaltoni, H., Mawad, M.E., Kakadiaris, I.A., 2010. Neck localization and geometry quantification of intracranial aneurysms. In: Proc. of IEEE International Symposium on Biomedical Imaging: From Nano To Macro. pp. 1057–1060.
- Shahzad, R., Pennig, L., Goertz, L., Thiele, F., Kabbasch, C., Schlamann, M., Krischek, B., Maintz, D., Perkhn, M., Borggrefe, J., 2020. Fully automated detection and segmentation of intracranial aneurysms in subarachnoid hemorrhage on CTA using deep learning. *Sci. Rep.* 10, 1–12.
- Shao, D., Lu, X., Liu, X., 2022. 3D intracranial aneurysm classification and segmentation via unsupervised dual-branch learning. *arXiv preprint arXiv:2201.02198*.
- Shi, Z., Miao, C., Schoepf, U.J., Savage, R.H., Dargis, D.M., Pan, C., Chai, X., Li, X.L., Xia, S., Zhang, X., et al., 2020. A clinically applicable deep-learning model for detecting intracranial aneurysm in computed tomography angiography images. *Nat. Commun.* 11, 1–11.
- Shimada, Y., Tanimoto, T., Nishimori, M., Choppin, A., Meir, A., Ozaki, A., Higuchi, A., Kosaka, M., Shimahara, Y., Kitamura, N., 2020. Incidental cerebral aneurysms detected by a computer-assisted detection system based on artificial intelligence: a case series. *Medicine* 99.
- Shit, S., Ezhov, I., Paetzold, J.C., Menze, B., 2020. Av-net: Automatic detection and segmentation of aneurysm. In: Proc. of International Workshop on Cerebral Aneurysm Detection. Springer, pp. 51–57.
- Sichtermann, T., Faron, A., Sijben, R., Teichert, N., Freiherr, J., Wiesmann, M., 2019. Deep learning-based detection of intracranial aneurysms in 3D TOF-MRA. *Am. J. Neuroradiol.* 40, 25–32.
- Sled, J.G., Zijdenbos, A.P., Evans, A.C., 1998. A nonparametric method for automatic correction of intensity nonuniformity in mri data. *IEEE Trans. Med. Imaging* 17, 87–97.
- Soler, J.P., Frangi, A.F., @neurIST Consortium, T., 2017. Database of cerebral artery geometries including aneurysms at the middle cerebral artery bifurcation. <http://dx.doi.org/10.15131/shef.data.4806910.v1>, URL [https://figshare.shef.ac.uk/articles/dataset/Database\\_of\\_Cerebral\\_Artery\\_Geometries\\_including\\_Aneurysms\\_at\\_the\\_Middle\\_Cerebral\\_Artery\\_Bifurcation/4806910](https://figshare.shef.ac.uk/articles/dataset/Database_of_Cerebral_Artery_Geometries_including_Aneurysms_at_the_Middle_Cerebral_Artery_Bifurcation/4806910).
- Song, M., Wang, S., Qian, Q., Zhou, Y., Luo, Y., Gong, X., 2024. Intracranial aneurysm cta images and 3d models dataset with clinical morphological and hemodynamic data. *Sci. Data* 11, 1213.
- Spuler, A., Goubergrits, L., 2020. CADA: Clinical background and motivation. In: Proc. of International Workshop on Cerebral Aneurysm Detection. Springer, pp. 21–28.
- Stafa, A., Leonardi, M., 2008. Role of neuroradiology in evaluating cerebral aneurysms. *Interv. Neuroradiol.* 14, 23–37.
- Stember, J.N., Chang, P., Stember, D.M., Liu, M., Grinband, J., Filippi, C.G., Meyers, P., Jambawalikar, S., 2019. Convolutional neural networks for the detection and measurement of cerebral aneurysms on magnetic resonance angiography. *J. Digit. Imaging* 32, 808–815.
- Štepán-Buksákovská, I., Accurso, J., Diehn, F., Huston, J., Kaufmann, T., Luetmer, P., Wood, C., Yang, X., Blezek, D., Carter, R., et al., 2014. Computer-aided diagnosis improves detection of small intracranial aneurysms on mra in a clinical setting. *Am. J. Neuroradiol.* 35, 1897–1902.
- Su, Z., Jia, Y., Liao, W., Lv, Y., Dou, J., Sun, Z., Li, X., 2020. 3D attention U-Net with pretraining: a solution to CADA-Aneurysm segmentation challenge. In: Proc. of International Workshop on Cerebral Aneurysm Detection. Springer, pp. 58–67.
- Sulayman, N., Al-Mawaldí, M., Kanafani, Q., 2016. Semi-automatic detection and segmentation algorithm of saccular aneurysms in 2D cerebral DSA images. *Egypt. J. Radiol. Nucl. Med.* 47, 859–865.
- Suniaga, S., Werner, R., Kemmling, A., Groth, M., Fiehler, J., Forkert, N.D., 2012. Computer-aided detection of aneurysms in 3D time-of-flight MRA datasets. In: Proc. of International Workshop on Machine Learning in Medical Imaging. Springer, pp. 63–69.
- Taha, A.A., Hanbury, A., 2015. Metrics for evaluating 3D medical image segmentation: analysis, selection, and tool. *BMC Med. Imaging* 15, 1–28.
- Taher, F., Mahmoud, A., Shalaby, A., El-Baz, A., 2018. A review on the cerebrovascular segmentation methods. In: Proc. of IEEE International Symposium on Signal Processing and Information Technology. ISSPIT, pp. 359–364.
- Thompson, J.D., 2015. The Role of the Free-Response Receiver Operating Characteristic Method for Dose and Image Quality Optimisation (Ph.D. thesis). University of Salford (United Kingdom).
- Timmins, K.M., van der Schaaf, I.C., Bennink, E., Ruigrok, Y.M., An, X., Baumgartner, M., Bourdon, P., De Feo, R., Di Noto, T., Dubost, F., et al., 2021. Comparing methods of detecting and segmenting unruptured intracranial aneurysms on TOF-MRAs: The ADAM challenge. *Neuroimage* 238, 118216.
- Timmins, K., van der Schaaf, I., Vos, I., Ruigrok, Y., Velthuis, B., Kuijff, H., 2022. Deep learning with vessel surface meshes for intracranial aneurysm detection. In: Proc. of Medical Imaging 2022: Computer-Aided Diagnosis. SPIE, pp. 633–637.
- Turan, N., Heider, R.A., Roy, A.K., Miller, B.A., Mullins, M.E., Barrow, D.L., Grossberg, J., Pradilla, G., 2018. Current perspectives in imaging modalities for the assessment of unruptured intracranial aneurysms: a comparative analysis and review. *World Neurosurg.* 113, 280–292.
- Turner, C.L., Kirkpatrick, P.J., 2000. Detection of intracranial aneurysms with unenhanced and echo contrast enhanced transcranial power doppler. *J. Neurol. Neurosurg. & Psychiatry* 68, 489–495.
- Uchiyama, Y., Ando, H., Yokoyama, R., Hara, T., Fujita, H., Iwama, T., 2006. Computer-aided diagnosis scheme for detection of unruptured intracranial aneurysms in MR angiography. In: Proc. of IEEE Engineering in Medicine and Biology. pp. 3031–3034.
- Ueda, D., Yamamoto, A., Nishimori, M., Shimono, T., Doihsita, S., Shimazaki, A., Katayama, Y., Fukumoto, S., Choppin, A., Shimahara, Y., et al., 2019. Deep learning for mr angiography: automated detection of cerebral aneurysms. *Radiology* 290, 187–194.
- van der Weide, R., Zuiderveld, K.J., Mali, W.T.M., Viergever, M.A., 1998. CTA-based angle selection for diagnostic and interventional angiography of saccular intracranial aneurysms. *IEEE Trans. Med. Imaging* 17, 831–841.
- Van Gijn, J., Kerr, R.S., Rinkel, G.J., 2007. Subarachnoid haemorrhage. *Lancet* 369, 306–318.
- Van Griethuysen, J.J., Fedorov, A., Parmar, C., Hosny, A., Aucoin, N., Narayan, V., Beets-Tan, R.G., Fillion-Robin, J.C., Pieper, S., Aerts, H.J., 2017. Computational radiomics system to decode the radiographic phenotype. *Cancer Res.* 77, e104–e107.
- Van Pelt, R., Gasteiger, R., Lawonn, K., Meuschke, M., Preim, B., 2014. Comparative blood flow visualization for cerebral aneurysm treatment assessment. pp. 131–140.
- Vaswani, A., Shazeer, N., Parmar, N., Uszkoreit, J., Jones, L., Gomez, A.N., Kaiser, L., Polosukhin, I., 2017. Attention is all you need. *Adv. Neural Inf. Process. Syst.* 30.
- Vlak, M.H., Algra, A., Brandenburg, R., Rinkel, G.J., 2011. Prevalence of unruptured intracranial aneurysms, with emphasis on sex, age, comorbidity, country, and time period: a systematic review and meta-analysis. *Lancet Neurol.* 10, 626–636.
- Wang, J., Sun, J., Xu, J., Lu, S., Wang, H., Huang, C., Zhang, F., Yu, Y., Gao, X., Wang, M., et al., 2023. Detection of intracranial aneurysms using multiphase CT angiography with a deep learning model. *Academic Radiol.* 30, 2477–2486.

- Wang, H., Zhang, J., 2022. A survey of deep learning-based mesh processing. *Commun. Math. Stat.* 10, 163–194.
- Weir, B., 2002. Unruptured intracranial aneurysms: a review. *J. Neurosurg.* 96, 3–42.
- Wermer, M.J., van der Schaaf, I.C., Algra, A., Rinkel, G.J., 2007. Risk of rupture of unruptured intracranial aneurysms in relation to patient and aneurysm characteristics: an updated meta-analysis. *Stroke* 38, 1404–1410.
- Wilson, D.L., Royston, D., Noble, J.A., Byrne, J.V., 1999. Determining X-ray projections for coil treatments of intracranial aneurysms. *IEEE Trans. Med. Imaging* 18, 973–980.
- Wong, W.C., Chung, A.C., 2006. Augmented vessels for quantitative analysis of vascular abnormalities and endovascular treatment planning. *IEEE Trans. Med. Imaging* 25, 665–684.
- Wong, S.C., Nawawi, O., Ramli, N., Abd Kadir, K.A., 2012. Benefits of 3D rotational DSA compared with 2D DSA in the evaluation of intracranial aneurysm. *Academic Radiol.* 19, 701–707.
- Woo, S., Park, J., Lee, J.Y., Kweon, I.S., 2018. Cbam: Convolutional block attention module. In: Proc. of the European Conference on Computer Vision. ECCV, pp. 3–19.
- Wood, D., Guilhem, E., Kafabadi, S., Busaidi, A.Al., Hammam, A., Mansoor, N., Townend, M., Agarwal, S., Wei, Y., Mazumder, A., et al., 2024. Automated brain abnormality detection using a self-supervised text-vision framework.
- Worthington, J.M., Goumas, C., Jalaludin, B., Gattellari, M., 2017. Decreasing risk of fatal subarachnoid hemorrhage and other epidemiological trends in the era of coiling implementation in australia. *Front. Neurol.* 8, 424.
- Wu, K., Gu, D., Qi, P., Cao, X., Wu, D., Chen, L., Qu, G., Wang, J., Pan, X., Wang, X., et al., 2022. Evaluation of an automated intracranial aneurysm detection and rupture analysis approach using cascade detection and classification networks. *Comput. Med. Imaging Graph.* 102, 102126.
- Yang, X., Blezek, D.J., Cheng, I.T., Ryan, W.J., Kallmes, D.F., Erickson, B.J., 2011. Computer-aided detection of intracranial aneurysms in mr angiography. *J. Digit. Imaging* 24, 86–95.
- Yang, X., Xia, D., Kin, T., Igarashi, T., 2020a. Intra: 3d intracranial aneurysm dataset for deep learning. In: Proc. of the IEEE/CVF Conference on Computer Vision and Pattern Recognition. pp. 2656–2666.
- Yang, X., Xia, D., Kin, T., Igarashi, T., 2020b. Surface-based 3D deep learning framework for segmentation of intracranial aneurysms from TOF-MRA images. arXiv preprint arXiv:2006.16161.
- Yang, X., Xia, D., Kin, T., Igarashi, T., 2023. A two-step surface-based 3d deep learning pipeline for segmentation of intracranial aneurysms. *Comput. Vis. Media* 9, 57–69.
- Yang, J., Xie, M., Hu, C., Alwalid, O., Xu, Y., Liu, J., Jin, T., Li, C., Tu, D., Liu, X., et al., 2021. Deep learning for detecting cerebral aneurysms with CT angiography. *Radiology* 298, 155–163.
- Ye, J., Xu, X., Li, L., Zhao, J., Lai, W., Zhou, W., Zheng, C., Wang, X., Lai, X., 2022. OTO-Net: An automated MRA image segmentation network for intracranial aneurysms. *Comput. Intell. Neurosci.* 2022.
- Yoon, N.K., McNally, S., Taussky, P., Park, M.S., 2016. Imaging of cerebral aneurysms: a clinical perspective. *Neurovasc. Imaging* 2, 1–7.
- Yu, J., Zhang, C., Wang, H., Zhang, D., Song, Y., Xiang, T., Liu, D., Cai, W., 2021. 3D medical point transformer: Introducing convolution to attention networks for medical point cloud analysis. arXiv preprint arXiv:2112.04863.
- Yuan, W., Peng, Y., Guo, Y., Ren, Y., Xue, Q., 2022. DCAU-Net: dense convolutional attention U-Net for segmentation of intracranial aneurysm images. *Vis. Comput. Ind. Biomed. Art* 5, 1–18.
- Zafar, Y., Javed, A., Malik, K.M., Santamaría, J., Malik, G., 2021. A diagnostic system for intracranial saccular and fusiform aneurysms with location detection. In: Proc. of IEEE EMBS International Conference on Biomedical and Health Informatics. BHI, pp. 1–4.
- Zakaria, H., Kurniawan, A., Mengko, T.L., Santoso, O.S., 2011. Detection of cerebral aneurysms by using time based parametric color coded of cerebral angiogram. In: Proc. of International Conference on Electrical Engineering and Informatics. pp. 1–4.
- Zeng, Y., Liu, X., Xiao, N., Li, Y., Jiang, Y., Feng, J., Guo, S., 2019. Automatic diagnosis based on spatial information fusion feature for intracranial aneurysm. *IEEE Trans. Med. Imaging* 39, 1448–1458.
- Zhao, H., Jiang, L., Jia, J., Torr, P.H., Koltun, V., 2021. Point transformer. In: Proceedings of the IEEE/CVF International Conference on Computer Vision. pp. 16259–16268.
- Zhou, J., Cui, G., Hu, S., Zhang, Z., Yang, C., Liu, Z., Wang, L., Li, C., Sun, M., 2020. Graph neural networks: A review of methods and applications. *AI Open* 1, 57–81.
- Zhou, E., Huang, F., 2022. Computer-assisted detection of intracranial aneurysms using a transformer deep neural network in 3D MR angiography.
- Zhou, Z., Jin, Y., Ye, H., Zhang, X., Liu, J., Zhang, W., 2024. Classification, detection, and segmentation performance of image-based AI in intracranial aneurysm: a systematic review. *BMC Med. Imaging* 24, 164.
- Zhou, Z., Siddiquee, M.M.R., Tajbakhsh, N., Liang, J., 2019c. Unet++: Redesigning skip connections to exploit multiscale features in image segmentation. *IEEE Trans. Med. Imaging* 39, 1856–1867.
- Zhou, Z., Sodha, V., Rahman Siddiquee, M.M., Feng, R., Tajbakhsh, N., Gotway, M.B., Liang, J., 2019d. Models genesis: Generic autodidactic models for 3d medical image analysis.
- Zhou, M., Wang, X., Wu, Z., Pozo, J.M., Frangi, A.F., 2019a. Aneurysm identification in cerebral models with multiview convolutional neural network. In: Proc. of International MICCAI Brainlesion Workshop. Springer, pp. 23–31.
- Zhou, M., Wang, X., Wu, Z., Pozo, J.M., Frangi, A.F., 2019b. Intracranial aneurysm detection from 3D vascular mesh models with ensemble deep learning. In: Proc. of Medical Image Computing and Computer-Assisted Intervention. Springer, pp. 243–252.
- Zhu, G., Luo, X., Yang, T., Cai, L., Yeo, J.H., Yan, G., Yang, J., 2022. Deep learning-based recognition and segmentation of intracranial aneurysms under small sample size. *Front. Physiol.* 13, 1084202.